Calhoun: The NPS Institutional Archive

DSpace Repository

Theses and Dissertations | 1. Thesis and Dissertation Collection, all items

1997-03

Metallization of CVD diamond using metal oxide intermediate layers for electronics packaging

Kroll, Darwin E

Monterey, California. Naval Postgraduate School

http://hdl.handle.net/10945/26062

Downloaded from NPS Archive: Calhoun

http://www.nps.edu/library

Calhoun is the Naval Postgraduate School's public access digital repository for research materials and institutional publications created by the NPS community. Calhoun is named for Professor of Mathematics Guy K. Calhoun, NPS's first appointed -- and published -- scholarly author.

Dudley Knox Library / Naval Postgraduate School
411 Dyer Road / 1 University Circle
Monterey, California USA 93943

NPS ARCHIVE
1997
KROLL, D.

NAVAL POSTGRADUATE SCHOOL
Monterey, California

THESIS

METALLIZATION OF CVD DIAMOND USING METAL OXIDE INTERMEDIATE LAYERS FOR ELECTRONICS PACKAGING

by

Darwin E. Kroll

March 1997

Thesis Co-Advisors: Indranath Dutta
Sarath Menon

Thesis
K86723

Approved for public release; distribution is unlimited.

DUDLEY KNOX LIBRARY
NAVAL POSTGRADUATE SCHOOL
MONTEREY CA 93943-5101

DUDLEY KNOX LIBRARY
NAVAL POSTGRADUATE SCHOOL
MONTEREY CA 93943-5101

REPORT DOCUMENTATION PAGE

Form Approved
OMB No. 0704-0188

Public reporting burden for this collection of information is estimated to average 1 hour per response, including the time for reviewing instruction, searching existing data sources, gathering and maintaining the data needed, and completing and reviewing the collection of information. Send comments regarding this burden estimate or any other aspect of this collection of information, including suggestions for reducing this burden, to Washington headquarters Services, Directorate for Information Operations and Reports, 1215 Jefferson Davis Highway, Suite 1204, Arlington, VA 22202-4302, and to the Office of Management and Budget, Paperwork Reduction Project (0704-0188) Washington DC 20503.

AGENCY USE ONLY *(Leave blank)*	2. REPORT DATE	3. REPORT TYPE AND DATES COVERED
	March 1997	Master's Thesis

4. TITLE AND SUBTITLE
METALLIZATION OF CVD DIAMOND USING METAL OXIDE INTERMEDIATE LAYERS FOR ELECTRONICS PACKAGING

5. FUNDING NUMBERS

6. AUTHOR(S)
Darwin E. Kroll

7. PERFORMING ORGANIZATION NAME(S) AND ADDRESS(ES)
Naval Postgraduate School
Monterey CA 93943-5000

8. PERFORMING ORGANIZATION REPORT NUMBER:

9. SPONSORING/MONITORING AGENCY NAME(S) AND ADDRESS(ES)

10. SPONSORING/MONITORING AGENCY REPORT NUMBER:

11. SUPPLEMENTARY NOTES
The views expressed in this thesis are those of the author and do not reflect the official policy or position of the Department of Defense or the US Government.

12a. DISTRIBUTION/AVAILABILITY STATEMENT
Approved for public release; distribution is unlimited.

12b. DISTRIBUTION CODE

13. ABSTRACT *(maximum 200 words)*

The high thermal conductivity of chemically vapor deposited CVD diamond (up to 2000 W/m/K) and its low dielectric constant (~5.6) makes it highly desirable for use as an electronics packaging substrate material. To make CVD diamond amenable to thick film metallization via standard industrial processes, a thin γ-alumina layer (~1500Å) was grown on diamond by reactive evaporation of Al in oxygen over a very thin Cr intermediate-layer (~700Å). Commercially available silver and gold thick films were applied to CVD diamond both with and without the metal-oxide inter-layer. The interfaces were characterized by scanning electron microscopy, energy dispersive x-ray spectroscopy, Auger electron spectroscopy and transmission electron microscopy. The intermediate oxide layer was found to result in well-adherent, chemically bonded interfaces between the metallization and the CVD diamond substrates for both Ag and Au pastes. Without the oxide layer, the Ag paste was found to have very poor adhesion to the substrate. The Au paste, developed for non-oxide substrates, was found to be nominally adherent to the CVDD substrate, although quantitative adhesion comparisons between the metallization with and without the oxide inter-layer was not obtained. Microstructural and chemical characterization studies of the interface suggest that the alumina layer enhances adhesion by producing chemically-reacted/solid-solution species across all interfaces and is therefore a very versatile approach for thick film metallization of CVDD.

14. SUBJECT TERMS	15. NUMBER OF PAGES:
CVD Diamond, Metallization, Electronics Packaging	65
	16. PRICE CODE

17. SECURITY CLASSIFICATION OF REPORT	18. SECURITY CLASSIFICATION OF THIS PAGE	19. SECURITY CLASSIFICATION OF ABSTRACT	20. LIMITATION OF ABSTRACT
Unclassified	Unclassified	Unclassified	UL

NSN 7540-01-280-5500

Standard Form 298 (Rev. 2-89)
Prescribed by ANSI Std. 239-18

Approved for public release; distribution is unlimited.

METALLIZATION OF CVD DIAMOND USING METAL OXIDE INTERMEDIATE LAYERS FOR ELECTRONICS PACKAGING

Darwin E. Kroll
Lieutenant, U.S. Navy
BSME, University of Utah, 1990

Submitted in partial fulfillment of the
requirements for the degree of

MASTERS OF SCIENCE IN MECHANICAL ENGINEERING

from the

NAVAL POSTGRADUATE SCHOOL
March 1997

nps Archive
1997.03
Kroll, D.

Thesis
K8723
c/2

DUDLEY KNOX LIBRARY
NAVAL POSTGRADUATE SCHOOL
MONTEREY CA 93943-5101

DUDLEY KNOX LIBRARY
NAVAL POSTGRADUATE SCHOOL
MONTEREY CA 93943-5101

ABSTRACT

The high thermal conductivity of chemically vapor deposited CVD diamond (up to 2000 W/m/K) and its low dielectric constant (~5.6) makes it highly desirable for use as an electronics packaging substrate material. To make CVD diamond amenable to thick film metallization via standard industrial processes, a thin γ-alumina layer (~1500Å) was grown on diamond by reactive evaporation of Al in oxygen over a very thin Cr intermediate-layer (~700Å). Commercially available silver and gold thick films were applied to CVD diamond both with and without the metal-oxide inter-layer. The interfaces were characterized by scanning electron microscopy, energy dispersive x-ray spectroscopy, Auger electron spectroscopy and transmission electron microscopy. The intermediate oxide layer was found to result in well-adherent, chemically bonded interfaces between the metallization and the CVD diamond substrates for both Ag and Au pastes. Without the oxide layer, the Ag paste was found to have very poor adhesion to the substrate. The Au paste, developed for non-oxide substrates, was found to be nominally adherent to the CVDD substrate, although quantitative adhesion comparisons between the metallization with and without the oxide inter-layer was not obtained. Microstructural and chemical characterization studies of the interface suggest that the alumina layer enhances adhesion by producing chemically-reacted/solid-solution species across all interfaces and is therefore a very versatile approach for thick film metallization of CVDD.

TABLE OF CONTENTS

I. INTRODUCTION 1

II. BACKGROUND 3
- A. DIAMOND IN ELECTRONICS PACKAGING 3
- B. CHEMICAL VAPOR DEPOSITED DIAMOND 5
- C. APPROACHES FOR TREATING THE CVDD SURFACE FOR METALLIZATION 8
- D. INTERFACES ASSOCIATED WITH FRITTED THICK PASTE METALLIZATION 9

III. EXPERIMENTAL DETAILS 13
- A. MATERIALS 13
- B. EXPERIMENTAL PROCEDURES 13

IV. RESULTS AND DISCUSSION 17
- A. BACKGROUND WORK ON Al_2O_3/Cr/CVDD 17
- B. METALLIZATION WITH SILVER PASTE 17
- C. METALLIZATION WITH GOLD PASTE 26
- D. EMBRITTLEMENT OF Au BY Pb-Sn SOLDER: A FAILURE ANALYSIS 43

V. SUMMARY AND CONCLUSIONS 45

REFERENCES 47

INITIAL DISTRIBUTION LIST 49

LIST OF FIGURES

Figure 1: Four major functions of the package. From [Ref. 2]. 4
Figure 2: Generalized schematic of the chemical processes occurring in a CVD diamond reactor. 7
Figure 3: CVD diamond film with <111> oriented growth direction. 8
Figure 4: CVD diamond film with <100> oriented growth direction. 8
Figure 5: Schematic of pull test used to measure peel strength of metallization. 16
Figure 6: Secondary electron image of Ag metallization (light) on <100> CVDD (dark) without inter-layer clearly showing cracking and peeling of Ag paste following firing to 400 °C. 18
Figure 7: Secondary electron image and the corresponding X-ray images (as noted on each figure) from Ag-metallization (3350 FERRO) layer on 75nm Cr/500nm Al_2O_3 layer on glass substrate. 20
Figure 8: Secondary electron images from interfacial region of Ag-metallization (3350 FERRO) layer on 60nm Cr/150nm Al_2O_3 layer on glass substrate. 21
Figure 9: Energy dispersive X-ray spectrum from the interfacial region of the Ag-metallized glass with Cr/Al_2O_3 inter-layer. 22
Figure 10: X-ray images from Ag-metallization (3350 FERRO) layer on 60nm Cr/150nm Al_2O_3 layer on glass substrate. 23
Figure 11: X-ray line scans from interfacial region of Ag-metallization (3350 FERRO) layer on 60nm Cr/150nm Al_2O_3 layer on glass substrate. 24
Figure 12: AES depth profile of Ag-metallized glass with Al_2O_3/Cr inter-layer showing inter-diffusion of Ag- Al_2O_3 and Al_2O_3-Cr layers. 26
Figure 13: Scanning electron micrograph showing sintering of Au particles, following firing, on the surface of the thick paste. 27
Figure 14: X-ray images from Au-metallization on CVDD substrate without inter-layer. 28
Figure 15: Secondary electron image and X-ray line scans from Au-metallization layer on CVDD substrate. X-axis is 3.4 μm long. 30
Figure 16: AES depth profile of Au-metallized CVDD substrate. 32
Figure 17: Secondary electron image and X-ray line scans from Au-metallization layer on 50nm Cr/165nm Al_2O_3 layer on CVDD substrate. X-axis is 3.2 μm long. 33
Figure 18: AES depth profiles of (a) Au- and (b) Ag-metallizations on CVDD with Al_2O_3/Cr inter-layer and AES depth profile of (c) Al_2O_3/Cr layer on CVDD [Ref. 1]. 36
Figure 19: Alumina/Cr film, annealed, showing (a) crystals of the alumina rich phase in the chromia rich phase; (b) Al elemental map; (c) O elemental map; (d) Al profile; (e) O profile. Profiles shown in (d) and (e) were obtained along a randomly drawn rectangle. 37
Figure 20: AES Survey from interfacial carbide layer of Au-metallization on CVDD with Al_2O_3/Cr inter-layer. 39

Figure 21: (a) Cr_3C_2 Auger [Ref. 24]; (b) $Cr_{23}C_6$ Auger peaks [Ref. 22]; (c) CVD diamond Auger peaks [Ref. 26]; and (d) C-Cr Auger peaks from Au-metallized CVDD with Cr/Al_2O_3 inter-layer 40
Figure 22: Cross-sectional TEM micrograph. region A represents the CVDD substrate, region B comprises the Al_2O_3/Cr layer as well as segregated glassy phases from the frits contained in the metallization, and region C represents the Au metal. EDX spectra from (b) interface between regions B and C; (c) mid-point of region C; and (d) region containing C-Cr crystallites at the interface between regions B and A..... 42
Figure 23: (a) Secondary electron image and (b) X-ray images of fracture surface of two Au pads revealing segregation of Pb and Sn at several near grain boundary regions.44

LIST OF TABLES

Table 1: Thermal conductivities compared..... 5
Table 2: Thermal and electrical properties of substrate materials compared. 5

ACKNOWLEDGMENTS

This research was supported by the Naval Surface Warfare Center-Crane Division, with Messrs. Kip Hoffer and Chris Sims as contract monitors.

The author would like to express his gratitude to the following for providing the CVD diamond substrates: Mr. Chris Sims of the Surface Warfare Center-Crane Division, Dr. Jake Sosniak of Naval Air Warfare Center, Indianapolis and Dr. Mike Drory of Crystallume Corporation.

The author would especially like to thank his family (Charlotte, Dar and Erika) for their love and support throughout this investigation.

I. INTRODUCTION

New circuit designs and new device structures have continuously met the ever-increasing demand for higher speed and higher density circuits. However, as a result of increasing circuit density and power applied to silicon chips, heat dissipation from the chips is becoming critical. In electronic devices, heat dissipation through the substrate is one of the best ways to achieve efficient thermal management for microcircuits. A highly thermal conductive substrate will enable heat to be readily dissipated from the chip. This is essential for high power transistors and multichip modules (MCMs).

Alumina (Al_2O_3) ceramic with a 25 W/m/K thermal conductivity at room temperature has been dominant among substrate materials. More recently, other highly thermal conductive substrates, which are made from silicon carbide (SiC) with a thermal conductivity of 270 W/m/K and aluminum nitride (AlN) ceramic with a thermal conductivity of 260 W/m/K, have been used. In the future, even greater thermal dissipation can be achieved by using chemically vapor deposited (CVD) diamond substrates with thermal conductivities as high as 2000 W/m/K.

From the standpoint of thermal conductivity and dielectric strength, diamond is the ideal substrate. It is however, difficult to metallize because of the inert nature of the surface of diamond. Common metallizations with high electrical conductivity such as Ag or Au do not adhere to it. Additionally, diamond's coefficient of thermal expansion is very small compared to Ag or Au, which results in large interfacial residual stresses between the substrate and the metallization.

The problems associated with the metallization of diamond have been addressed through a unique approach, which modifies the surface of CVD diamond with a very thin and continuous alumina layer [Ref. 1]. This thesis continues the investigation of that system with its primary emphasis being on the characterization of the interfaces and the actual metallization of the system using both Ag and Au pastes.

II. BACKGROUND

A. DIAMOND IN ELECTRONICS PACKAGING

Electronics packaging is the, "...science and the art of establishing interconnections and a suitable operating environment for predominantly electrical circuits to process or store information" [Ref. 2]. Electronic packages contain many electrical circuit components, notably resistors, capacitors, diodes, and transistors. To form circuits these components need interconnections. Individual circuits must also be connected with each other to form functional units. Mechanical support and protection are required for those units. To function, electrical circuits need to be supplied with electrical energy, which is consumed and transformed into thermal energy. Because all circuits operate best within a limited temperature range, packaging must offer an adequate means for removal of heat. This leads to the four major functions of an electronics package, i.e., power distribution, signal distribution, heat dissipation, and circuit protection as illustrated in Figure 1.

Multichip electronics packaging technology has received widespread attention in the electronics industry. The use of multichip modules (MCMs) promises to increase packaging density and system performance beyond what is otherwise possible through the use of VLSI and surface mount technology. As in the case of most advanced technologies, the drive towards high performance MCMs has given rise to a number of engineering and materials challenges. In advanced MCMs where high speed, high power chips are mounted in close proximity on large circuit boards, heat spreading and removal

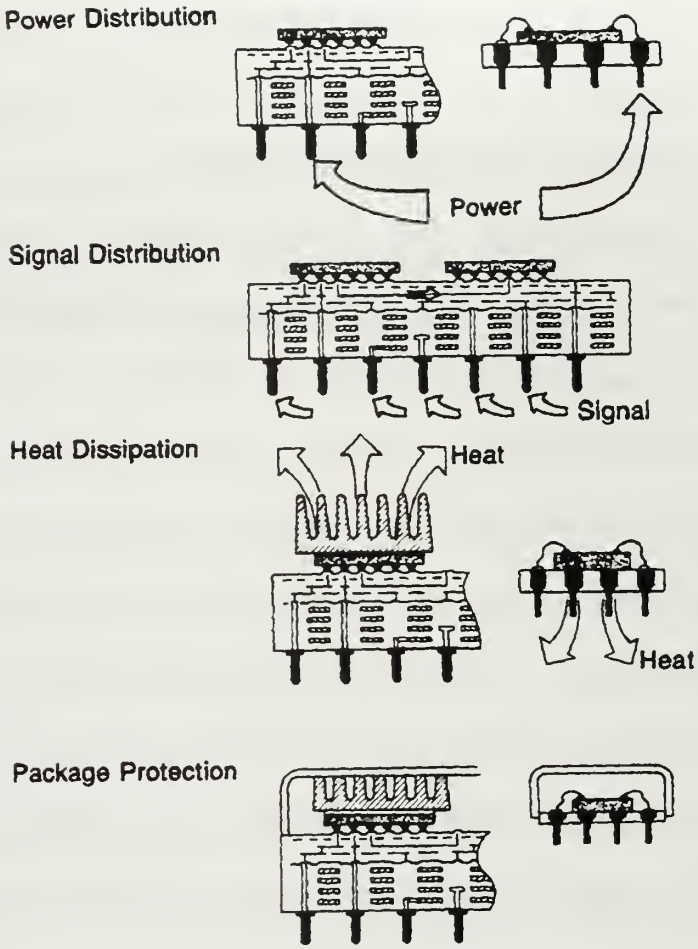

Figure 1: Four major functions of the package. From [Ref. 2].

become major issues. Diamond has the highest known thermal conductivity and at the same time is an electrical insulator. It holds great promise in solving thermal management problems in MCMs. The use of diamond substrates may also make possible the use of three-dimensional MCMs. Some common materials and their corresponding thermal conductivities are listed in Table 1. It is important to notice that there are no materials even close to diamond in thermal conductivity.

Material	Conductivity (Watts/m/K)
Diamond Natural IIa	2300
CVD Diamond	1400-2000
Water	581
Silver	418
Copper	393
Gold	311
Silicon carbide	270
Aluminum nitride	260
Aluminum	238
Silicon	150
Platinum	71
Chromium	66
Gallium arsenide	46
Alumina	25
Kovar	17
Epoxy-Kevlar	2

Table 1: Thermal conductivities compared.

Diamond has other attractive material properties. These properties are listed and compared in Table 2.

Material	CTE [$x10^{-6}$/ K]	Dielectric Constant	Electrical Resistivity [Ω cm]	Loss Tangent
CVD Diamond	~1-2	5.6	10^{13} - 10^{16}	0.0005
Silicon Carbide	3.4	42	$>10^{14}$	-
Aluminum Nitride	4.5	8.8	10^{11} - 10^{14}	0.06
Alumina	7	8.5	10^{8} - 10^{9}	0.004

Table 2: Thermal and electrical properties of substrate materials compared.

B. CHEMICAL VAPOR DEPOSITED DIAMOND

Substrate materials are chosen on the basis of dielectric strength, thermal conductivity, thermal expansion and surface finish. Substrate material choices have essentially been limited to plastics, aluminum oxide and to a much lesser extent AlN, SiC and glass ceramics. Alumina ceramics are the most widely used substrates for both thin- and thick-film hybrid circuits and MCMs [Ref. 3]. With increasing thermal load of

integration of active devices, substrate materials with better thermal conductivity need to be developed. Because of its excellent thermal conductivity (k), diamond is believed to be the ideal material for the next generation of electronics packages. In addition to high k, diamond possesses high electrical resistivity ($>10^{13}$ Ω cm) and a low dielectric constant (5.6). It is also the hardest and most chemically inert of all known materials. However, the high cost of natural type IIa diamond makes it prohibitively expensive for electronics packaging applications. During the last several decades, however, methodologies for producing synthetic diamond have been developed, substantially reducing the costs involved. The first experiment on CVD of synthetic diamond was reported in 1956 by B. V. Derjaguin et al. [Ref. 4] who synthesized diamond from the gas phase and grew it on non-diamond substrates. In 1979, Sedaka and his group in Japan were able to deposit diamond on diamond surfaces using thermal cracking of methane gas [Ref. 5]. In 1982, they succeeded in depositing diamond on the surfaces of silicon, molybdenum and silica. Research on the gas phase synthesis of diamond has progressed very rapidly. Recently, there has been considerable progress in the preparation of diamond and diamond-like films and even of free-standing diamond substrates using several different methods of gas phase synthesis including plasma enhanced chemical vapor deposition (Figure 2) and magnetically enhanced dc-arc jet deposition process. The advent of these current methods has brought the price of synthetic diamond down

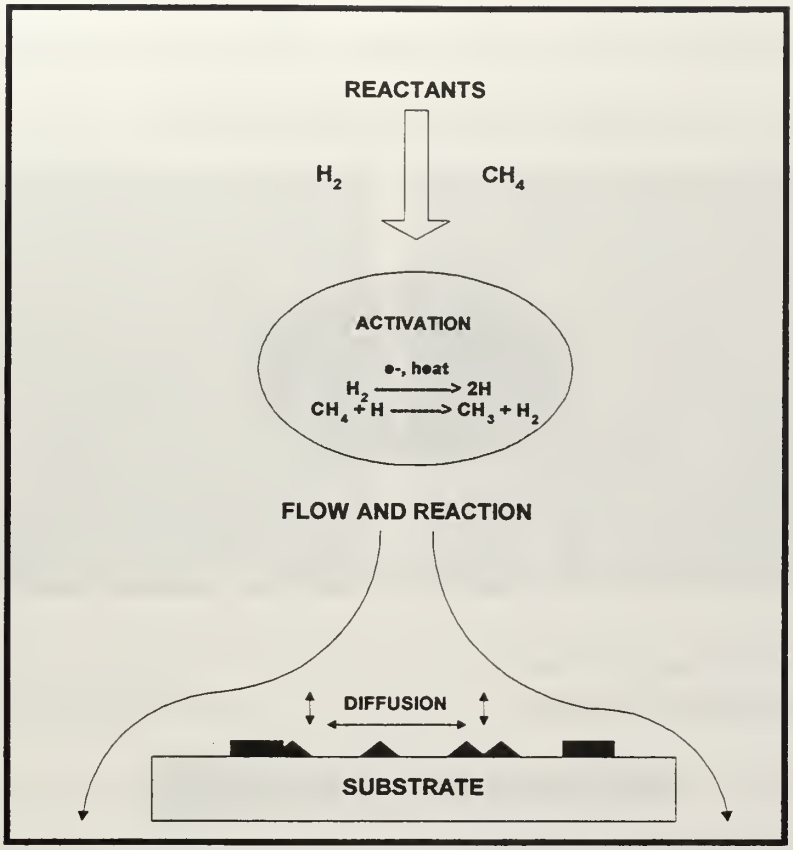

Figure 2: Generalized schematic of the chemical processes occurring in a CVD diamond reactor.

considerably. A great deal of the motivation to develop synthetic diamond has come from the hard facing industry in which drill bits, blades, and machine tools are coated with diamond to create tools with superior characteristics to the conventional surface hardening treatments previously employed. Diamond is grown in the <111> direction for hard facing applications and <100> for electronics packaging. The <111> direction of diamond is the direction of the strong sp3 hybrid orbital bonds and is consequently harder. Interestingly, that it is also the direction of highest thermal conductivity. The <100> face is softer and therefore easier to polish and thus utilized in electronics

packaging applications. Figures 3 and 4 show scanning electron micrographs of CVD diamond with <111> and <100> growth directions, respectively.

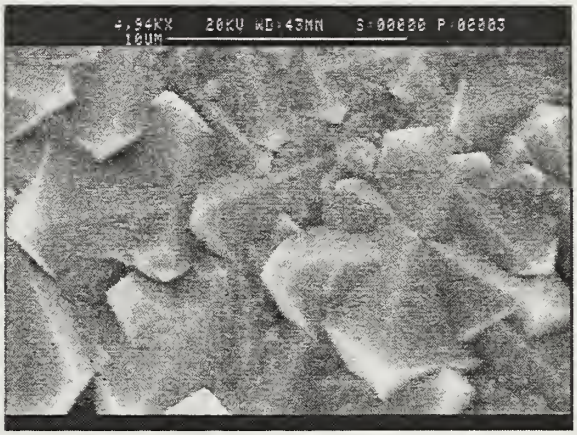

Figure 3: CVD diamond film with <111> oriented growth direction.

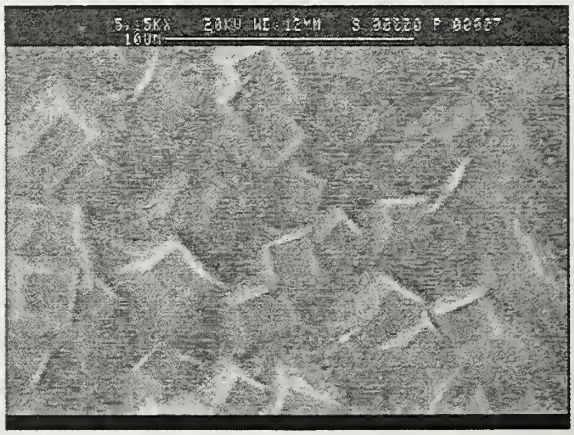

Figure 4: CVD diamond film with <100> oriented growth direction.

C. APPROACHES FOR TREATING THE CVDD SURFACE FOR METALLIZATION

Although diamond is an excellent substrate material for thermal management, diamond is difficult to metallize. The inert nature of the surface of diamond makes it difficult for common metallizations with high electrical conductivity such as Ag or Au to adhere to it. The second difficulty is due to its small, compared to Ag or Au, thermal expansion coefficient (~1-2 x 10^{-6}/K), which results in large interfacial residual stresses between the substrate and the metallization. Traditional approaches to metallize diamond have utilized less electrically conductive, but carbide-forming metals (W, Mo, Nb, or Ti) with smaller thermal expansion mismatch with diamond than Ag or Au, as either the final metallization, or an inter-layer between Ag or Au, metallizations and diamond [Ref. 6] and [Ref. 7]. Carbide-forming metals usually have less than ideal electrical conductivity,

and are therefore not very desirable as the final conductive metallization. When used as an inter-layer, it had to be patterned identically to the overlying interconnection circuitry, since a continuous metallic inter-layer between the CVD diamond and the metallization would short out the circuitry. Additionally, using the carbide-forming metal as an inter-layer, in practice precludes this approach from being used for conventional thick film processes [Ref. 8].

D. INTERFACES ASSOCIATED WITH FRITTED THICK PASTE METALLIZATION

Thick films are used extensively in electronic circuits to provide low resistance circuit interconnections, resistor and capacitor terminations, and external connector bonding pads. The following discussion on thick pastes is based on Refs. [Ref. 9] and [Ref. 10] Thick film conducting metallization pastes are usually composed of a metallic conductive component comprising one or more precious metals in fine powder form, a bonding agent comprising fine glass frit and/or metal oxide, and an organic suspension medium. The basic adhesion mechanism of the film to the substrate is provided by the glass frits. The metallic and glass frit components are initially suspended in the organic medium. The paste flows through the pattern screen onto the substrate and is dried. During the drying process much of the volatile suspension medium is eliminated. The glass frits have not melted and the metallic particles are still unsintered. The patterns are then fired to a high temperature. The firing cycle consists of a warm up period during which the remainder of the organic suspension medium is eliminated by volatilization or by burning off to form carbon dioxide or carbon monoxide. This is followed by a short period at peak firing temperature. At the peak firing temperature, glass frits melt and

flow to rearrange the metallic conductive components. The metallic particles are suspended in the molten glassy phase and are drawn together by capillary action and are sintered to form the conductive circuit. Too much glass phase results in metallic clusters within pools of the glass melt and too little glass results in incomplete rearrangement of the metallic particles because of insufficient capillary forces since the metallic particles are not completely wetted. Of note, a fritted paste may have better electrical conductivity than if the paste were composed of only pure conducting metal particles in the organic suspension. Following the rearrangement of the metallic conducting particles, liquid-phase sintering further increases the density of the conducting circuit. Some grain growth and shape accommodation takes place as well as elimination of any remaining pores from the organic suspension medium that may still be present within the pattern. The pattern continues to cool slowly, annealing the film.

Bonding of the metallization to the substrate material is accomplished by both wetting the surface and infiltration of the grain boundaries at the surface. This results in primarily mechanical interlocking. Frits can be chosen so that not only do they wet the surface but also will chemically bond with the substrate material. This can result in stronger bonding than mechanical interlocking alone [Ref. 11]. As can be seen from the above discussion, the selection of glass frit and volume fraction to use in a conducting thick film is dependent on the precious metal of the paste and the substrate material.

Two thick film pastes, one Ag and the other Au, were used in the current work. Review of the literature [Ref. 12] and [Ref. 13] shows that sustained heating up to 1000 °C in a vacuum or an inert gas does not lead to any noticeable diamond graphitization but that in the presence of atomic oxygen, a black graphitic-like coating may be detected on

the diamond surface at temperatures as low as 625 °C [Ref. 14]. Since the recommended firing temperature of the Au paste used in this work was 800 °C, the thermal stability of the CVDD substrate was tested by heating it in flowing argon in a tube furnace and held at 825 °C for 35 minutes. Subsequent SEM examination of the sample surface revealed that the crystallite facets were still distinct. The thermal stability was then tested to 1000 °C at which point the facets began to show disintegration.

III. EXPERIMENTAL DETAILS

A. MATERIALS

The CVD diamond substrates were produced and provided by Naval Air Warfare Center (<100> oriented CVDD on AlN and Si) and Crystallume Inc. (<111> oriented CVDD on Si and Ti). Additional samples were provided by Naval Surface Warfare Center, Crane Division (freestanding <100> oriented CVDD samples). All CVDD substrates were produced using plasma enhanced chemical vapor deposition (PECVD).

The Cr used for evaporation was obtained from Ernest F. Fullam Inc. and had a purity level of 99.99%. The aluminum used for reactive evaporation was obtained from The Aldrich Chemical Company and had a purity level of 99.999%. The oxygen used for reactive evaporation was 99.99% pure. The Ag thick paste was provided by Ferro and is trademark name Conductrox-3350. The Au thick paste is DC101 from Dupont Electronic Materials, which was experimental at the time but is currently marketed as product 5771.

B. EXPERIMENTAL PROCEDURES

The experimental apparatus consisted of a HV system equipped with two thermal evaporation sources, a substrate heater with type K thermal couple, film thickness monitor and gas feed-through for back filling with O_2.

The substrate samples were sectioned using a slow speed saw with diamond wafering blade. After sectioning the samples were cleaned by soaking in acetone for 20 minutes, rinsed with methanol and then dried. The substrates were then clamped to a combination sample holder/heater assembly in the vacuum chamber and baked at 370 °C for a period of four-to-six hours in a base pressure of 2×10^{-7} torr. Following substrate

baking an approximately 60 nm thick layer of Cr was deposited at a deposition rate of 4 nm/min. Following the deposition of the Cr, oxygen was bled into the chamber to obtain a pressure of 5×10^{-4} torr. 150nm of aluminum was then reactively evaporated onto the Cr coated substrate. The chamber was subsequently back-filled with oxygen to a pressure of 500 torr and the freshly deposited Al-O film was annealed at 400 °C for 24 - 48 hours in order to produce stoichiometric nanocrystalline γ–Al_2O_3 [Ref. 15].

Following surface modification of the CVDD substrates, some of them were metallized using thick, fritted Ag and Au pastes. The pastes were stirred thoroughly and then were spread over the entire sample using a rubber spatula. This procedure produced a uniform film thickness of 15-20 microns, and a complete and continuous coverage of the surface was obtained. After metallization, the samples were dried at 150 °C for ten minutes and then fired in the tube furnace using the appropriate firing temperature profile for the metallization paste (Ag: heating rate of 19 °C/min, 12 minutes at a peak temperature of 400 °C, 18 °C/min descent rate; Au: heating rate of 22 °C/min, 10 minutes above 840 °C with peak at 855 °C, 17.5 °C/min descent rate).

Following surface modification and metallization as outlined above, the various interfaces within the sample were analyzed by scanning electron microscopy (SEM), Auger electron spectroscopy (AES), and transmission electron microscopy (TEM).

For cross-sectional SEM, the edge of the metallized sample was metallographically polished to a finish of 1 μm, following which a combination of backscattered electron imaging (BSI) and energy dispersive x-ray spectroscopy (EDXS) with a 100 nm probe size were utilized to characterize the concentration profiles across

the interfaces. In addition, secondary electron imaging, where necessary, was utilized to characterize the sample surface.

Metallized samples were analyzed using AES. Depth profiles were obtained using one-minute sputter intervals. Energy windows were set for Au (1995-2035 eV), Ag (335-365 eV), Al (1375-1405 eV), O (492-520 eV), Cr (517-540 eV), C (254-287 eV), Pb (2160-2205 eV), and Zn (975-1005 eV). Detailed surveys covering the range from 0-2000 eV were then obtained at interfaces and other key depths.

All TEM analysis was done on a TOPCON OO2B transmission electron microscope using 200kV acceleration voltage with both 6nm and 4nm probe sizes for EDXS.

Pull testing to measure the adhesive strength of the substrate-metallization interface was conducted as listed in section 30.1.2.4 of military standard MIL-M-28787D and was conducted by Naval Surface Warfare Center, Crane Division. A schematic of the test is shown in Figure 5. Five test coupons were prepared and sent to Crane for testing. They consisted of two <100> coupons (one with the Cr/Al_2O_3 inter-layer and one without), two <111> coupons (one with the Cr/Al_2O_3 inter-layer and one without), and one 99.6% pure Al_2O_3 coupon for comparison. Due to the high thermal conductivity of the CVD diamond substrate, the Au pads were over heated during soldering. This resulted in the embrittlement of the pads due to diffusion of Pb and Sn along the Au grain boundaries and the consequent formation of intermetallics. At soldering temperature (~160 °C), Pb-Sn solder rapidly dissolves large quantities of gold. The resulting intermetallic is hard, brittle and porous [Ref. 16]. SEM and EDXS revealed intermetallic particles on the fracture surfaces of the pads, as discussed later.

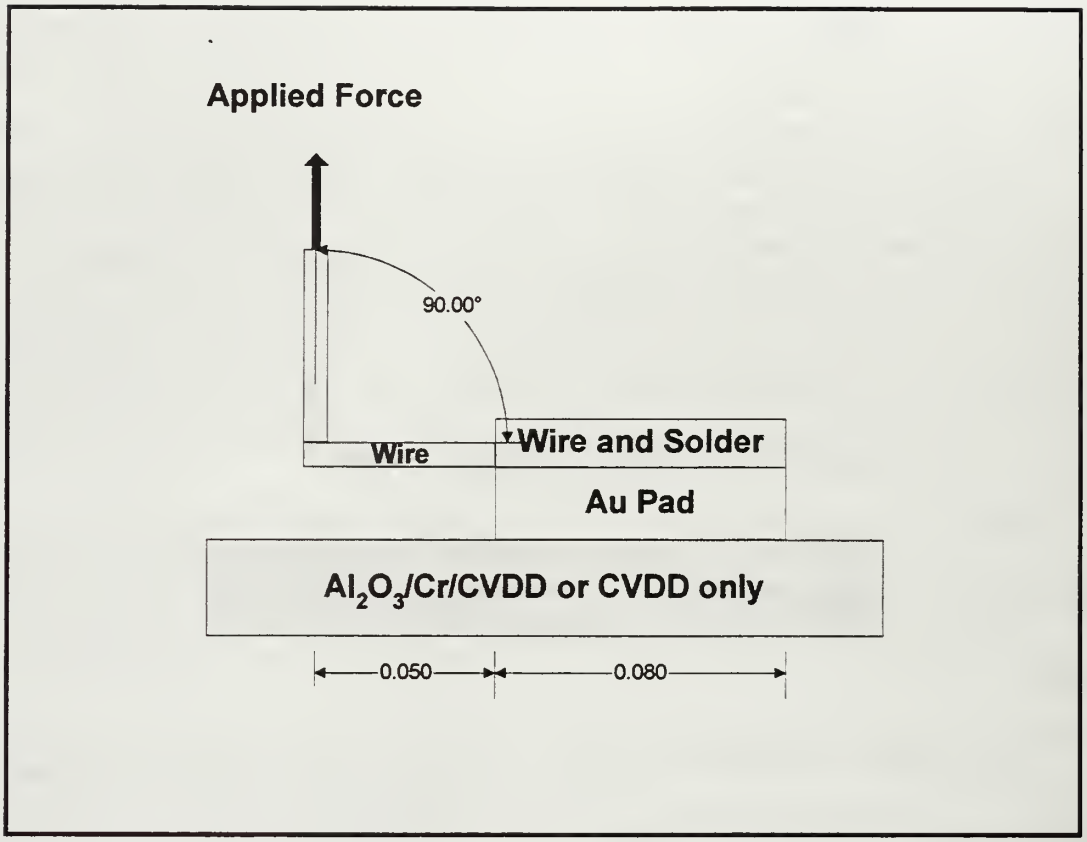

Figure 5: Schematic of pull test used to measure peel strength of metallization.

IV. RESULTS AND DISCUSSION

A. BACKGROUND WORK ON Al_2O_3/Cr/CVDD

Details of the surface modification of CVDD by producing a thin adherent alumina film can be found in reference 1. An alumina layer was produced [Ref. 1] on a CVD diamond substrate by the process described in section III-B. A brief synopsis of this study is provided below.

1. Specific resistance of the films were > 180 Ω•cm.
2. Selected area diffraction (SAD) patterns, in the transmission electron microscope (TEM), showed that the crystal structure of the films was identical to γ-Al_2O_3.
3. Bright field imaging of the film showed fine 3-10 nm sized grains of alumina.
4. Auger electron spectroscopy further confirmed that the surface layer, was indeed alumina. No metallic Al was found in the samples.
5. Auger depth profiles revealed that there was interdiffusion between the Cr and C as well as between the Cr and both Al and O. The Cr interlayer provided adhesion enhancement of the alumina layer to the CVD diamond by chemical bonding.
6. The adhesive strength of the modification was qualitatively evaluated by use of acetate packaging tape. The alumina films were found to be adherent.

B. METALLIZATION WITH SILVER PASTE

First, a <100> oriented CVD diamond substrate was metallized directly using the Ag thick paste without any intermediate layer. The recommended firing profile for the paste was followed as described in section III-B. The Ag paste was cracked and peeled when retrieved from the furnace after firing (Figure 6). The paste was easily wiped off and the metallization was deemed non-adherent. The paste, containing oxide frits, was designed for oxide substrates; so the lack of adhesion was not unexpected since no

chemical bonding was established between the CVDD and the liquid oxide phases formed during the firing treatment.

Figure 6: Secondary electron image of Ag metallization (light) on <100> CVDD (dark) without inter-layer clearly showing cracking and peeling of Ag paste following firing to 400 °C.

Subsequently, two glass substrates with the Al_2O_3/Cr surface modification were metallized using the Ag thick paste. One sample had a 500nm Al_2O_3 layer over a 75nm

Cr layer while the other had a 150nm Al_2O_3 layer over a 60nm Cr layer. Visual inspection of the paste following firing revealed that it was uncracked and had not peeled off from either sample. The adhesive strength of the film was tested using acetate packaging tape. The film adhered to the alumina layer and could not be pulled off. Cross-sectional samples were prepared for characterization of the different interfaces with the SEM. The SE image (Figure 7; top left panel) shows the microstructure and the O Kα, Al Kα, Pb Mβ, Ag Lα and the Cr Kα X-ray images are presented in subsequent panels in Figure 7. The layer has sharp interfaces as seen in the X-ray images. The Al Kα image (left middle panel) and the O Kα image (top right panel) clearly indicates that the Al_2O_3 layer deposited on the Cr layer (see Cr Kα image; bottom right panel) is intact even after curing the metallization at 400 °C. The oxygen signal (upper right panel) coincides with both the Al and the Pb signals with different intensities, indicating that the Al_2O_3 is stable to the metallization heat treatment and a layer rich in lead-oxide forms between the Al_2O_3 and the Ag layer. The FERRO 3350 paste also contains other elements like Cd, Zn, Si, etc. in smaller quantities and are also distributed within the Ag layer or the Pb oxide rich layer. The Pb signal (middle right panel) shows segregation of Pb between the Ag and Al regions, indicating that the PbO-rich phase formed at the alumina/metallization interface during firing.

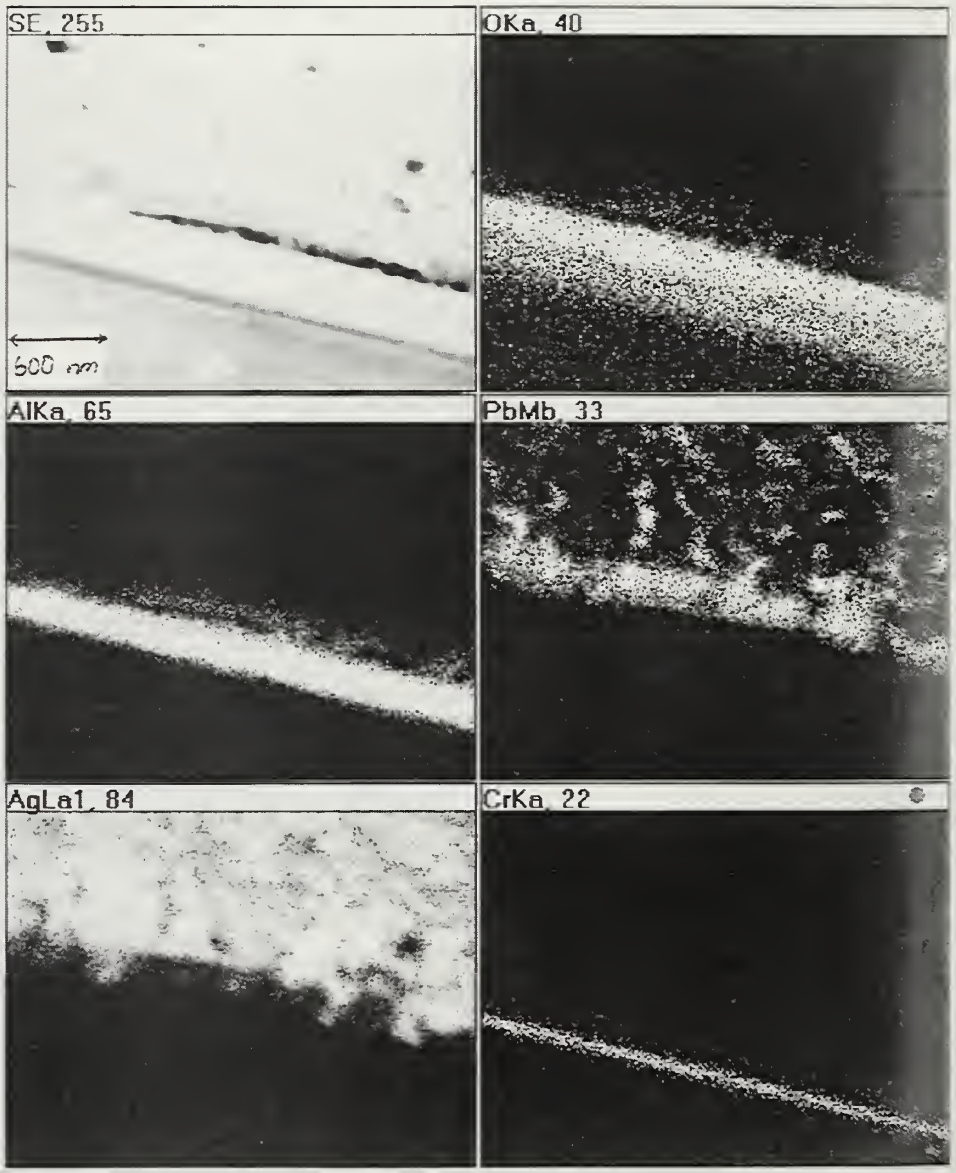

Figure 7: Secondary electron image and the corresponding X-ray images (as noted on each figure) from Ag-metallization (3350 FERRO) layer on 75nm Cr/500nm Al_2O_3 layer on glass substrate.

Another example showing the effect of metallization heat treatment on the Cr/Al_2O_3 thin film is presented in Figure 8. Here, the secondary electron image (top left) clearly shows the Ag layer and the Cr/Al_2O_3 layer on the glass substrate (dark area on left side of Figure 8). In addition, it can also be seen that there is another layer in between the Ag layer and the Cr/Al_2O_3 , which formed during the metallization heat treatment and is indicated as the reacted layer.

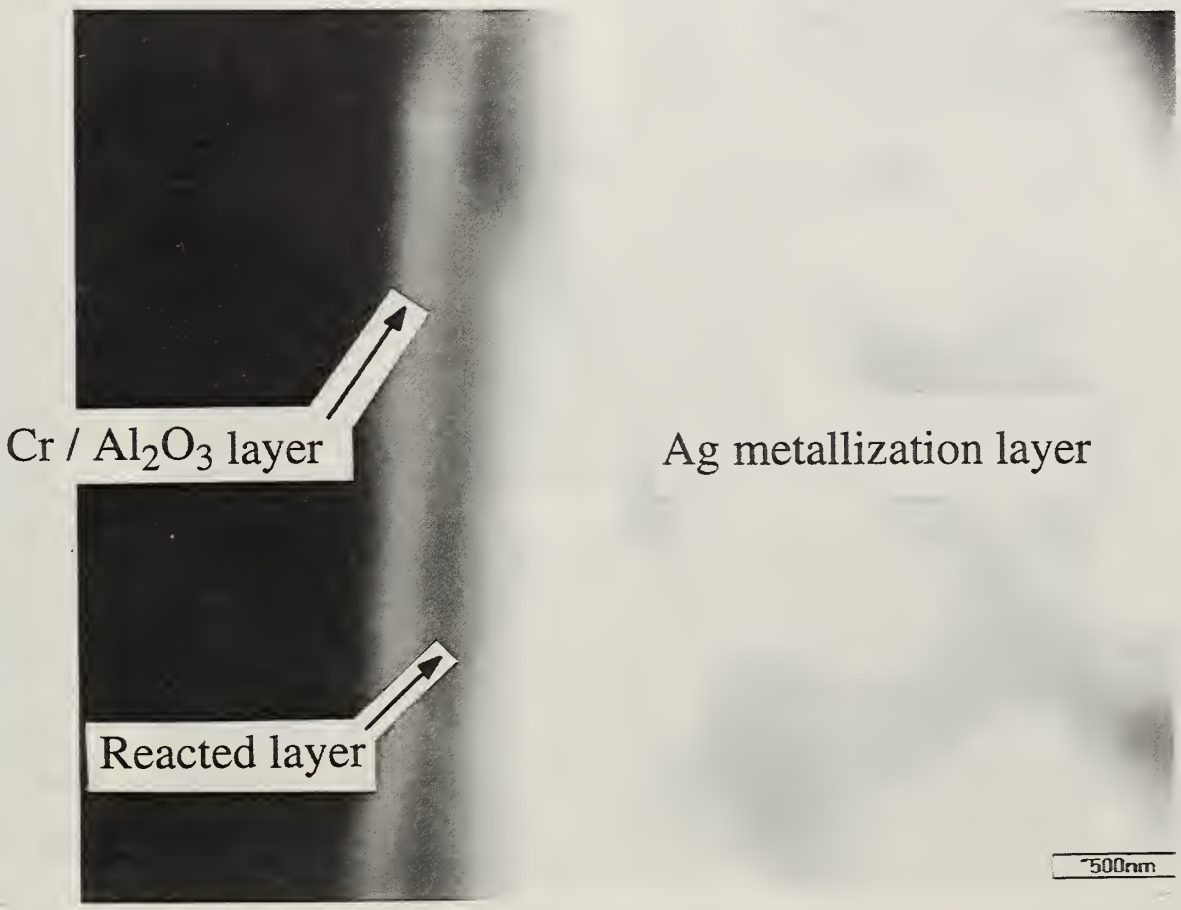

Figure 8: Secondary electron images from interfacial region of Ag-metallization (3350 FERRO) layer on 60nm Cr/150nm Al_2O_3 layer on glass substrate.

Typical X-ray spectrum obtained from the central position of Figure 8 is illustrated in Figure 9 clearly indicating the presence of Al, Cr, Pb, Cd, Ag and O.

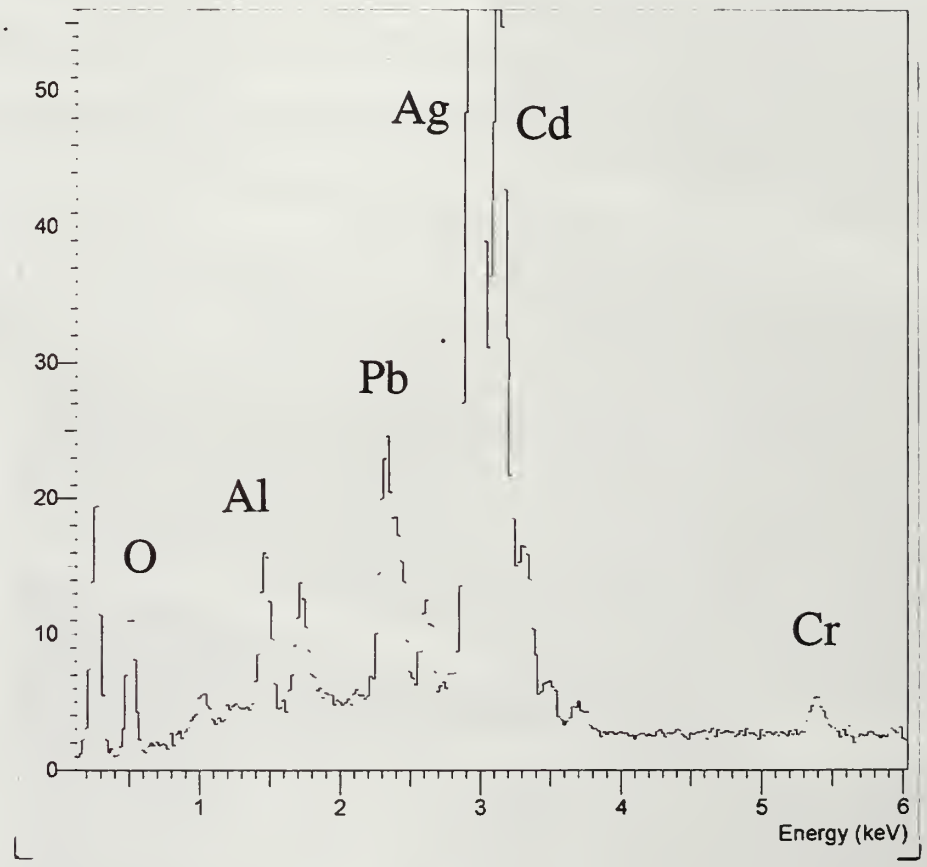

Figure 9: Energy dispersive X-ray spectrum from the interfacial region of the Ag-metallized glass with Cr/Al_2O_3 inter-layer.

X-ray images (Figure 10) from the 150nm Al_2O_3/60nm Cr sample also show distinct Cr and Al layers. The Ag film also contains Cd oxide frits. In the lower left panel the Cd signal is seen. Noticeably absent is the concentration of Cd at the interface with Al_2O_3 as was seen with the Pb. What is seen is that the Cd signal appears uniform throughout the region indicating that it is present in a lesser amount than the Pb oxide and

that it is primarily used to bond with the Ag and the Pb oxide but not necessarily to wet the substrate surface.

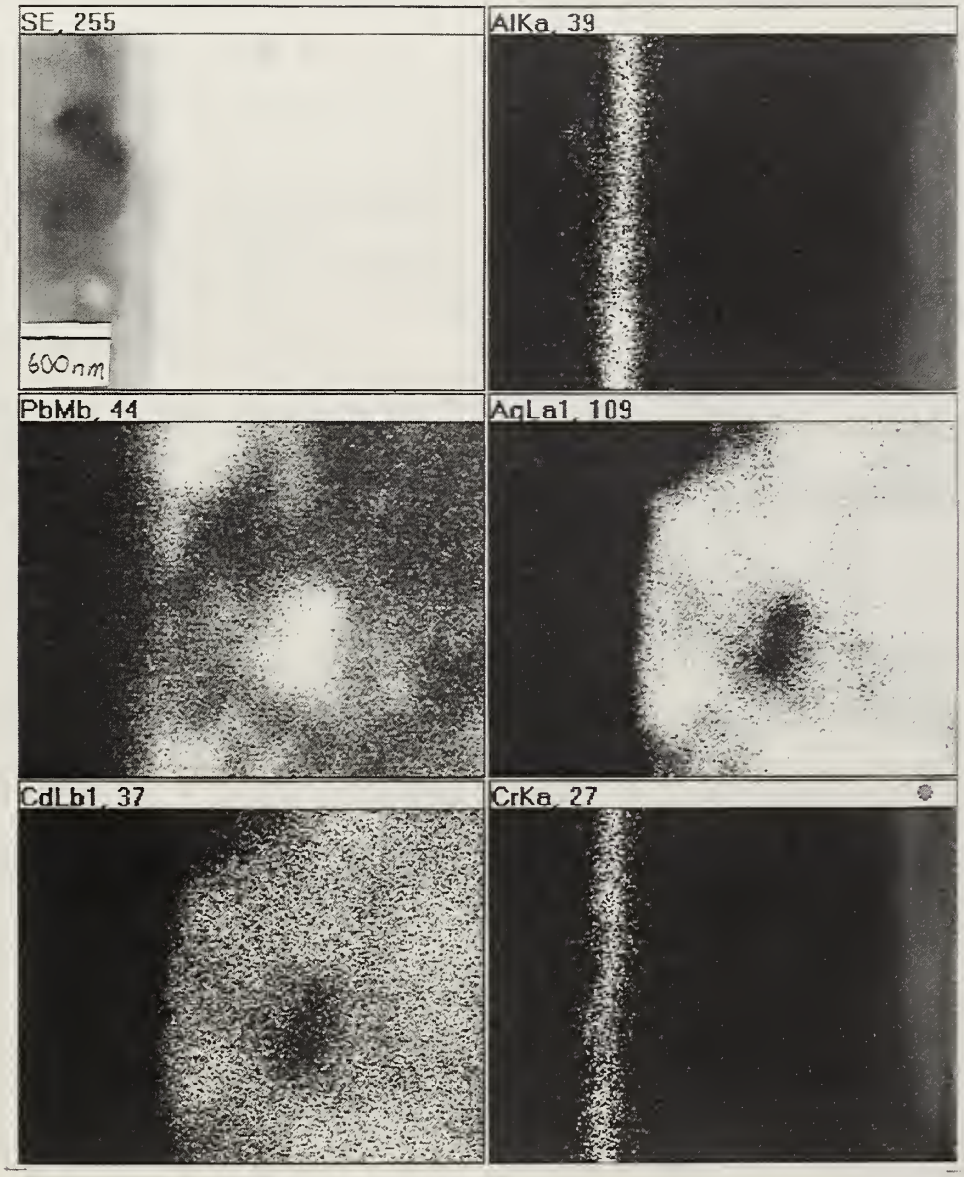

Figure 10: X-ray images from Ag-metallization (3350 FERRO) layer on 60nm Cr/150nm Al_2O_3 layer on glass substrate.

X-ray line scans (Figure 11) from the 150nm Al_2O_3/60nm Cr sample show that there are distinct Cr and Al layers. The concentration of the Pb at the Al interface is also shown. The line scans clearly show evidence of interdiffusion across the Cr/Al interface, the Al/Pb interface, and the Pb/Ag interface. The Cd signal matches the signal for Ag.

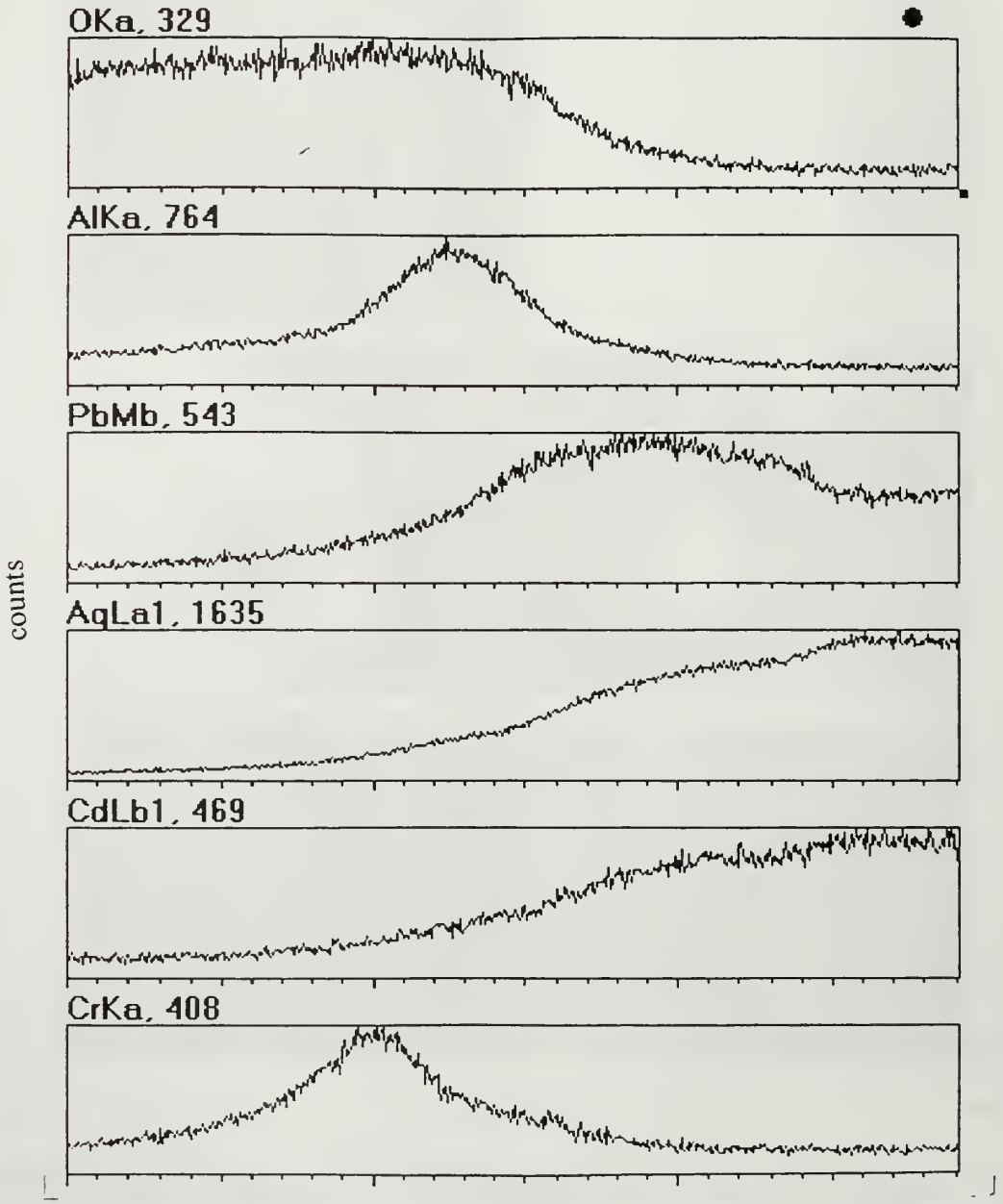

Figure 11: X-ray line scans from interfacial region of Ag-metallization (3350 FERRO) layer on 60nm Cr/150nm Al_2O_3 layer on glass substrate.

The X-ray images discussed above provide a qualitative indication of the elemental distribution following the metallization treatment. However, it must be remembered that the electron beam excited volume in the SEM is quite large relative to the thicknesses of the Al_2O_3 and Cr layers, and inferences about the extent of inter-diffusion that occurred across the various layers in these samples can not be made. Auger electron spectroscopy and depth profile analysis (by ion sputtering) were carried out to evaluate the elemental distribution with sub-nm resolution. At the same time, chemical bonding information could also be obtained from the energies of various Auger transitions and Auger peak profiles.

The AES depth profile (Figure 12) also shows interdiffusion at the various interfaces suggesting strong bonding between the Ag, Al_2O_3 and Cr layers. The oxygen signal and the aluminum signal are very similar indicating that all of the Al is reacted and in the form of Al_2O_3. Based on the above results, it can be inferred that although the Ag-metallization does not bond well to the diamond directly, it shows evidence of good chemical bonding on to the Al_2O_3/Cr layer, suggesting that it will adhere well to CVDD coated with Al_2O_3 and Cr (since, in reference 1, the Cr/Al_2O_3 layer has been shown to adhere to CVDD).

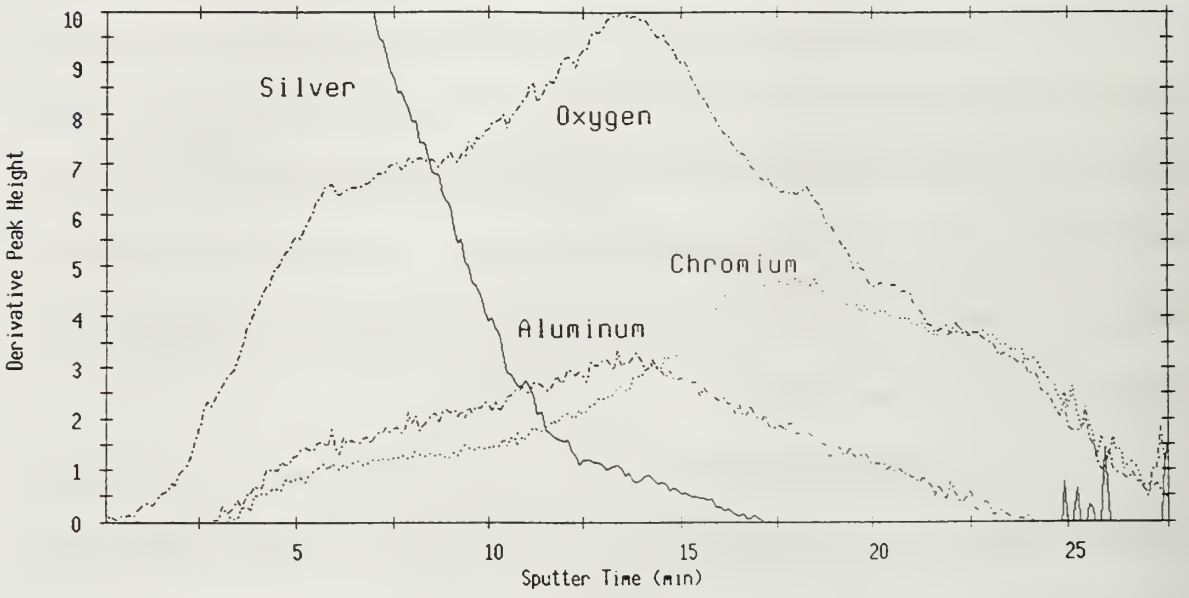

Figure 12: AES depth profile of Ag-metallized glass with Al_2O_3/Cr inter-layer showing inter-diffusion of Ag- Al_2O_3 and Al_2O_3-Cr layers.

C. METALLIZATION WITH GOLD PASTE

<100> oriented CVD diamond substrates were metallized with Au paste, both with and without the Al_2O_3/Cr inter-layer. The typical appearance of the as-fired Au is shown in Figure 13. Examination of the exposed edges of diamond in the scanning electron microscope revealed that they had not undergone oxidation, indicating that the argon environment had protected the CVD diamond and was conducive to good firing of the Au paste.

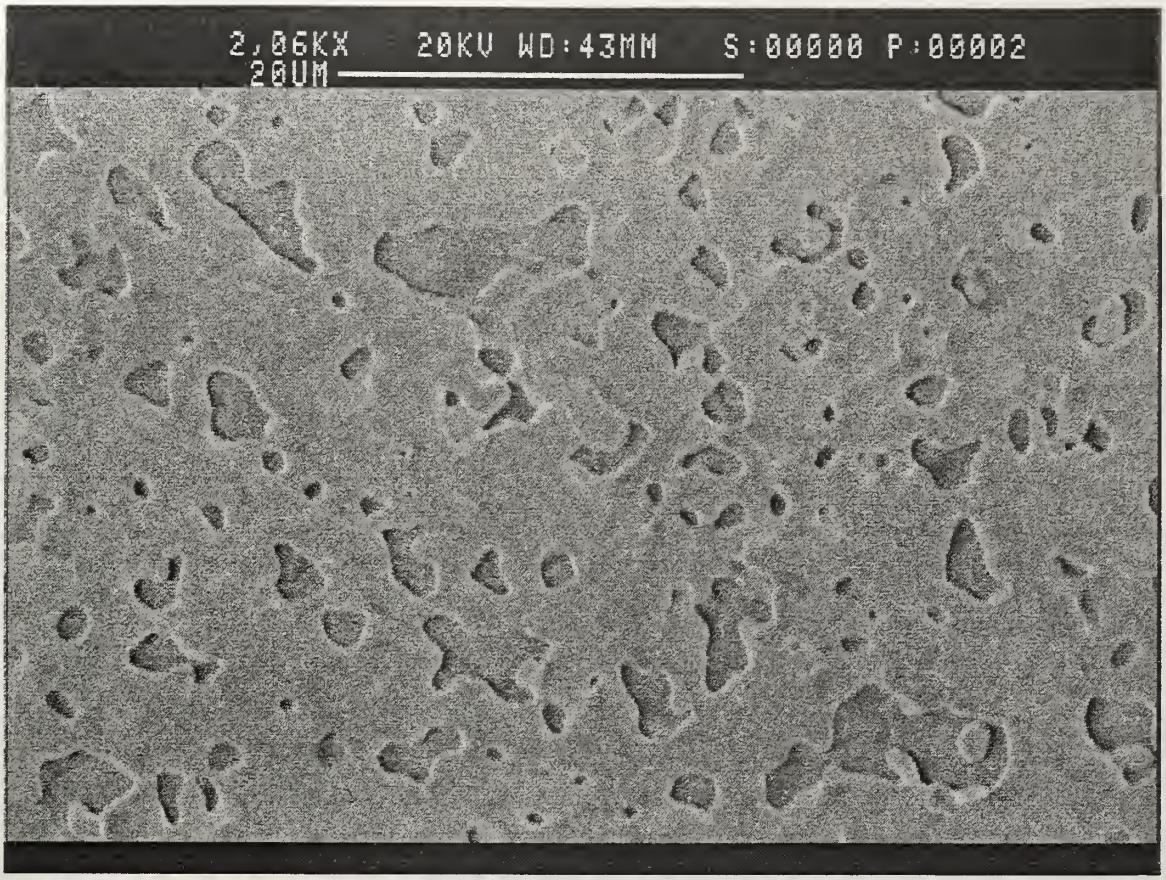

Figure 13: Scanning electron micrograph showing sintering of Au particles, following firing, on the surface of the thick paste.

The cross-sections of the metallized samples were analyzed by SEM and EDXS. The elemental x-ray maps for the Au-metallized CVDD sample without the Al_2O_3/Cr inter-layer are shown in Figure 14. Some oxygen segregation is observed between the underlying AlN and CVDD, possibly due to surface oxides present on AlN prior to CVDD deposition. There is also a slight concentration of oxygen, along with Si on the surface of the diamond, suggesting segregation of the Si-O glass frit present in the paste on the surface of the CVD diamond. The two bottom panels show the Au and Cu signals that make up the bulk of the remaining thick paste composition. A concentration of the

Au signal is observed in the region where Si and O are also concentrated, suggesting there may be a Si-Au-O compound/solid-solution present.

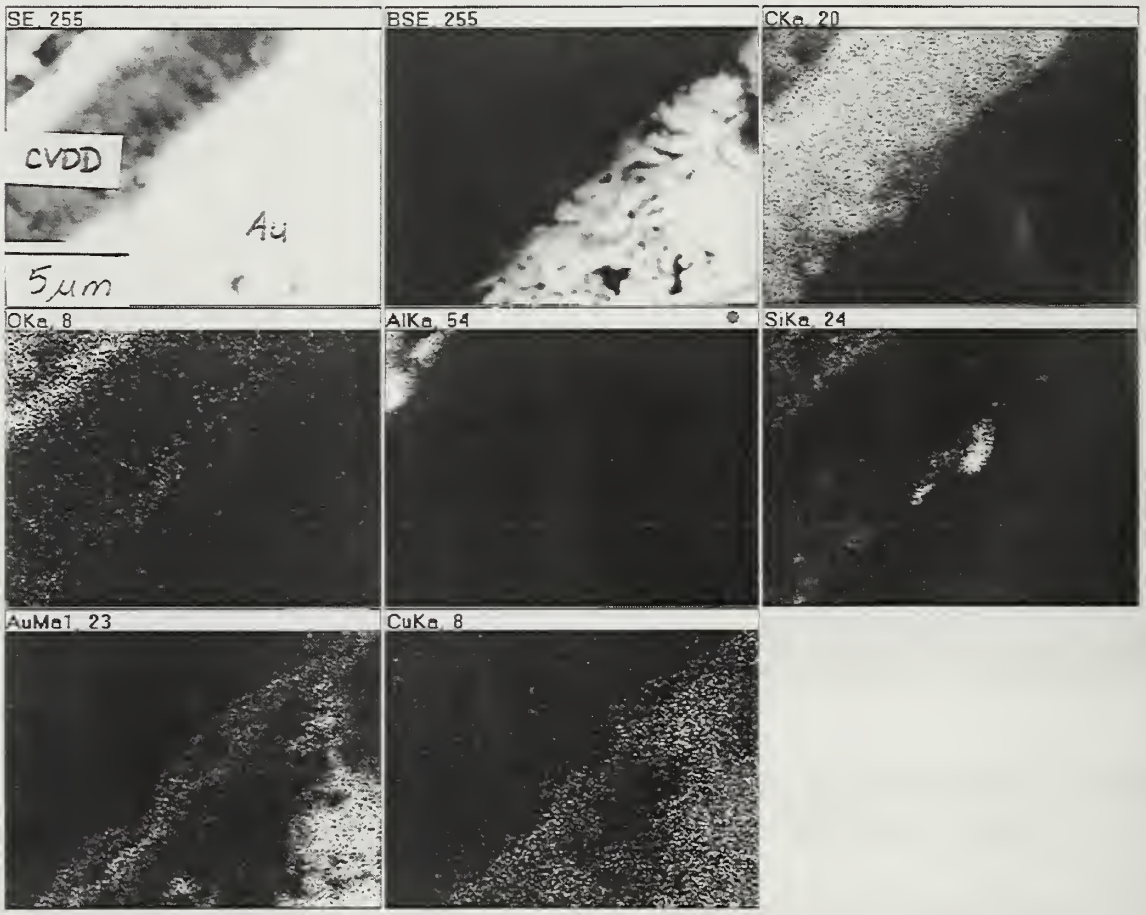

Figure 14: X-ray images from Au-metallization on CVDD substrate without inter-layer.

Figure 15 shows the SE image of the same interface (Au on CVDD without inter-layer) and shows the x-ray line scans across the interface. A rise in the oxygen and Si signals is seen at the interface. This is most likely from the Si-O frit present in the paste, which melted during firing and segregated to the diamond surface. There is a rise in the Au signal just after the rise in the Si and O signals indicating a possible Si-Au-O

compound or solid solution. Beyond the Si-Au-O interface layer, the Au signal rises in conjunction with the rise of the Cu signal. Together, they comprise the conductive circuit layer. The drop seen in all of the component signals on the far right side of the line scans is due to the presence of a hole.

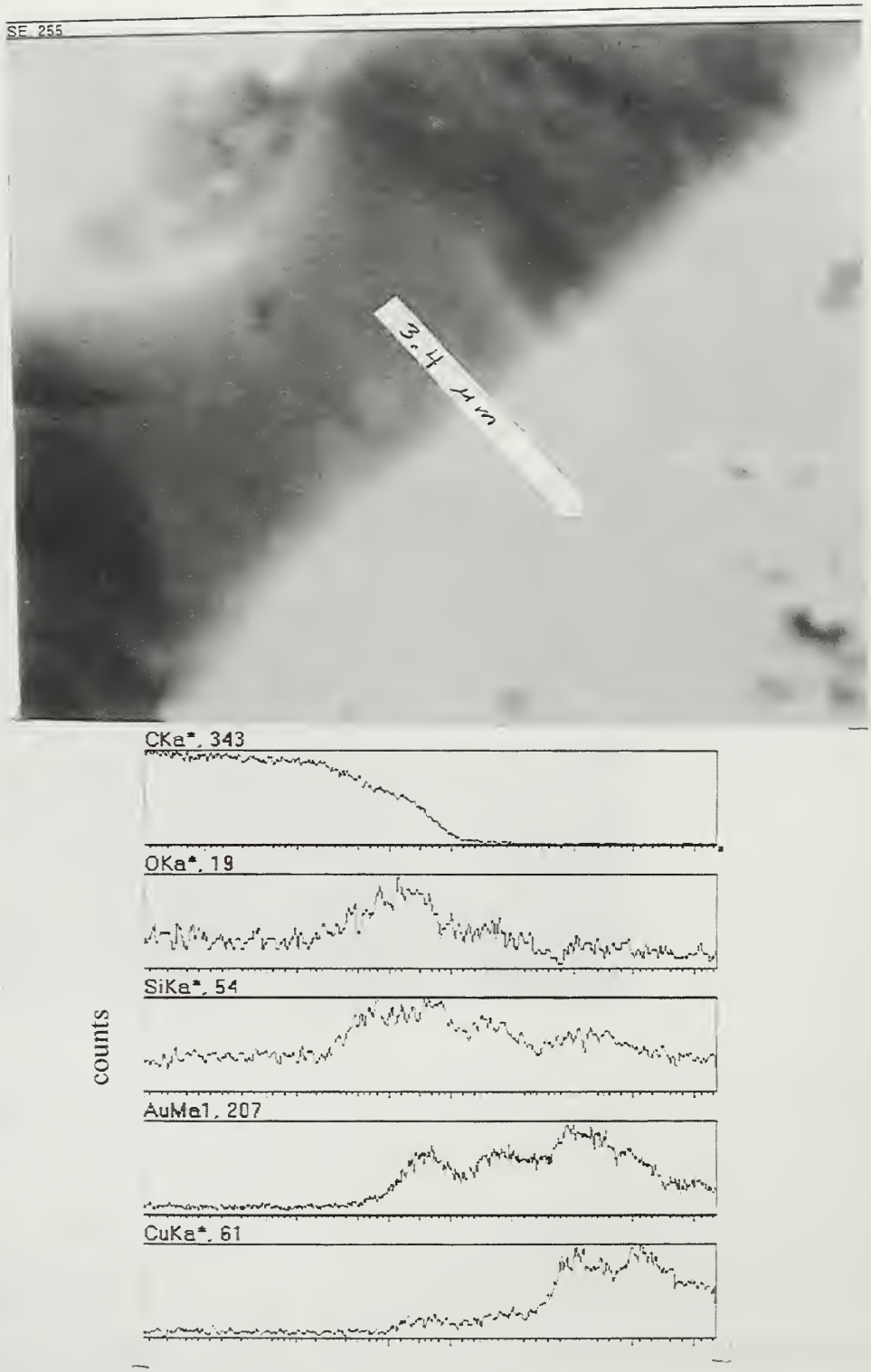

Figure 15: Secondary electron image and X-ray line scans from Au-metallization layer on CVDD substrate. X-axis is 3.4 μm long.

The AES depth profile shown in Figure 16 shows the elemental concentration variations at the interface of the diamond and the Au paste without Al_2O_3/Cr inter-layer. It appears that some intermixing between the C, Au and the Si-O layer that separate them (indicated by the oxygen signal) has occurred. However, it should be noted that the Auger signals were collected from an area about 30 μm x 30 μm in size. Since this was much larger than the average {100} diamond crystal face, it is likely that the elemental signals in Figure 16 did not all come from the same depth. The (100) crystal faces, as shown in Figure 4, are typically separated by some empty space, allowing any liquid glassy phase produced during the firing of the metallization to penetrate into these spaces and thereby produce mechanical interlocking effects. The overlapping of the Au and the C signals observed in Figure 16 is at least partly attributable to the fact that the recorded Auger electrons originated from different depths in the sample. It is well known that Au and C do not have affinity towards each other, and therefore it is unlikely that the interfacial region containing chemically intermixed Au and C. More detailed experiments with a smaller probe size than the CVDD crystallite size are needed in order to verify the nature of the interfacial region.

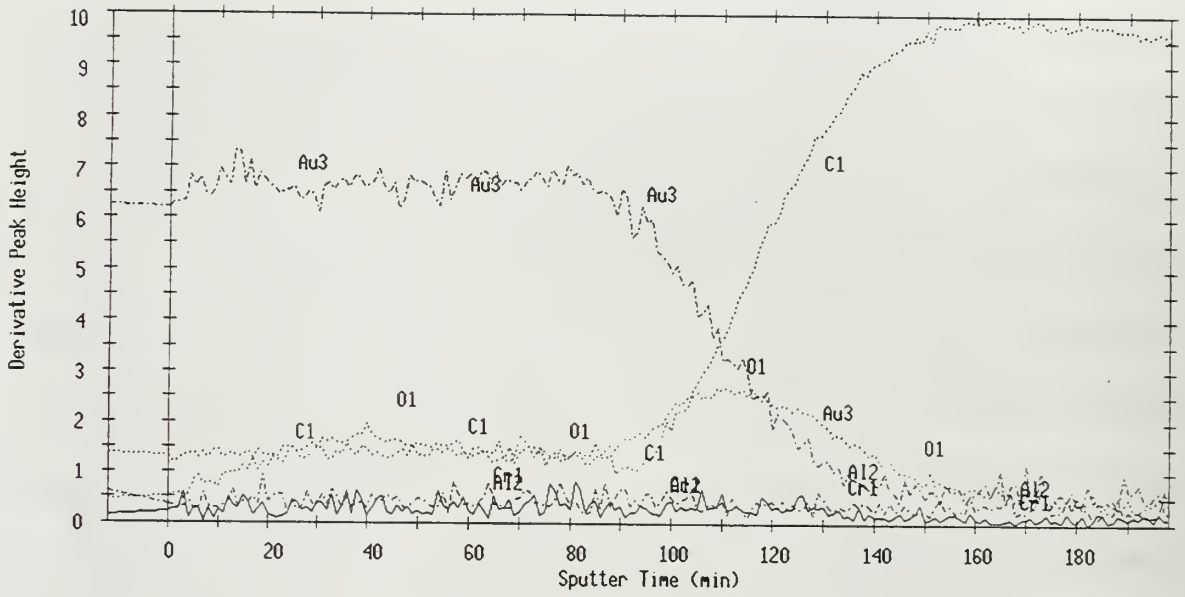

Figure 16: AES depth profile of Au-metallized CVDD substrate.

Figure 17 shows the SE image of the cross-section of the Au-metallized CVDD with Al_2O_3/Cr inter-layer and shows the x-ray line scans across the interfaces. Deep in the paste region there are strong signals from Au and Cu. Si and O show distinct peaks located between the Au and the Al_2O_3. It is not possible to resolve the extent of diffusion at the interfaces associated with the Al_2O_3/Cr inter-layer because of the tear drop effect associated with x-ray generation in a SEM sample. The range of x-ray generation for Al in Al_2O_3 with a 20 keV acceleration voltage is 4.5 μm [Ref. 17] and the as deposited Al_2O_3 layer is only 165 nm. It is, however, possible to determine that the Al and Cr layers are still present and distinct.

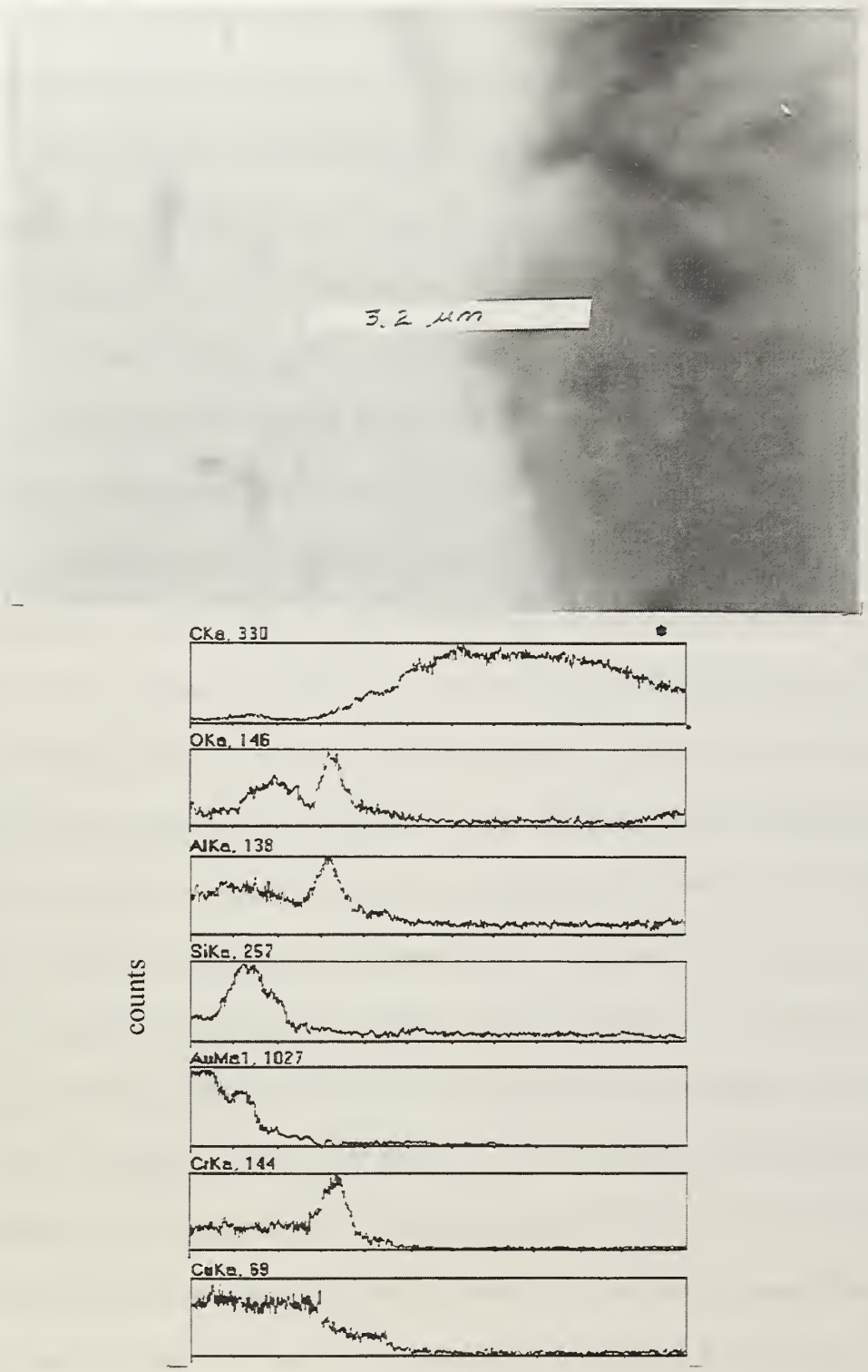

Figure 17: Secondary electron image and X-ray line scans from Au-metallization layer on 50nm Cr/165nm Al_2O_3 layer on CVDD substrate. X-axis is 3.2 μm long.

The AES depth profiles (Figures 18a, b and c) show the elemental concentrations through the thickness of the Au-metallized, Ag-metallized and unmetallized samples, respectively. It is observed that the Cr peak is aligned with the Al and O peaks in the Au-metallized sample suggesting that during firing of the metallization at 840 °C, there was appreciable inter-diffusion between the Cr and alumina layer. This is in contrast with the unmetallized and Ag-metallized samples (Figures 18b and 18c) where the Cr and Al peaks were separated. The migration of the Cr peak towards the Al peak in Figure 18a is partially explained by examination of the Cr_2O_3/Al_2O_3 phase diagram [Ref. 18] and [Ref. 19] which shows that Cr_2O_3 and Al_2O_3 form a solid solution at all compositions and that there is a miscibility gap within the solid solution region. The annealing process following deposition of Cr and Al/O results in the diffusional mixing of Cr, Al and O. Figures 19a through 19e show a bright field TEM image and PEELS (parallel electron energy loss spectroscopy) elemental maps of Al and O in the resultant microstructure [Ref. 20]. The Al-L elemental map shown in Figure 19(b) shows a uniform distribution of Al rich regions in Figure 19(a). The composition modulation of Al seen in Figure 19(b) and in the line profile in Figure 19(d) and uniformity of oxygen in the microstructure suggests that the composition of the Cr/Al_2O_3 thin film falls within the miscibility gap and two phases, one rich in Al_2O_3 and the other depleted in Al_2O_3 (and hence rich in Cr_2O_3) coexist in the microstructure. The increased firing temperature of the Au paste causes an increase in the rate of diffusion resulting in the intermixing of Al and Cr. A plot of the intensity in Figure 19(b) is shown in Figure 19(d) and clearly indicates that the microstructure contains alternating Al-rich and Al-poor regions. The O-K elemental map (Figure 19(c)) shows that O is uniformly distributed in the

microstructure. The O line profile (Figure 19(e)) demonstrates the uniformity in O concentration in the microstructure.

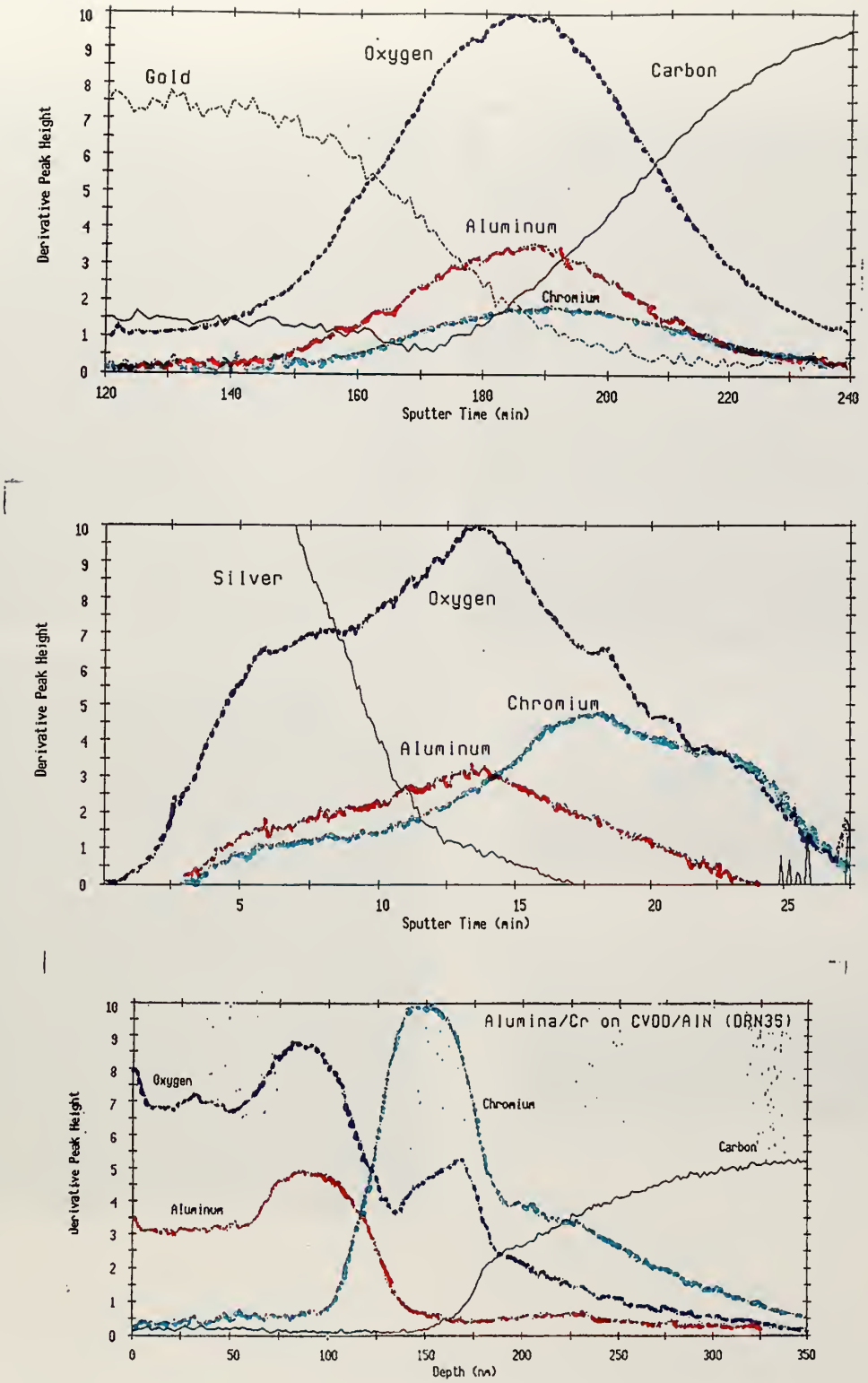

Figure 18: AES depth profiles of (a) Au- and (b) Ag-metallizations on CVDD with Al_2O_3/Cr inter-layer and AES depth profile of (c) Al_2O_3/Cr layer on CVDD [Ref. 1].

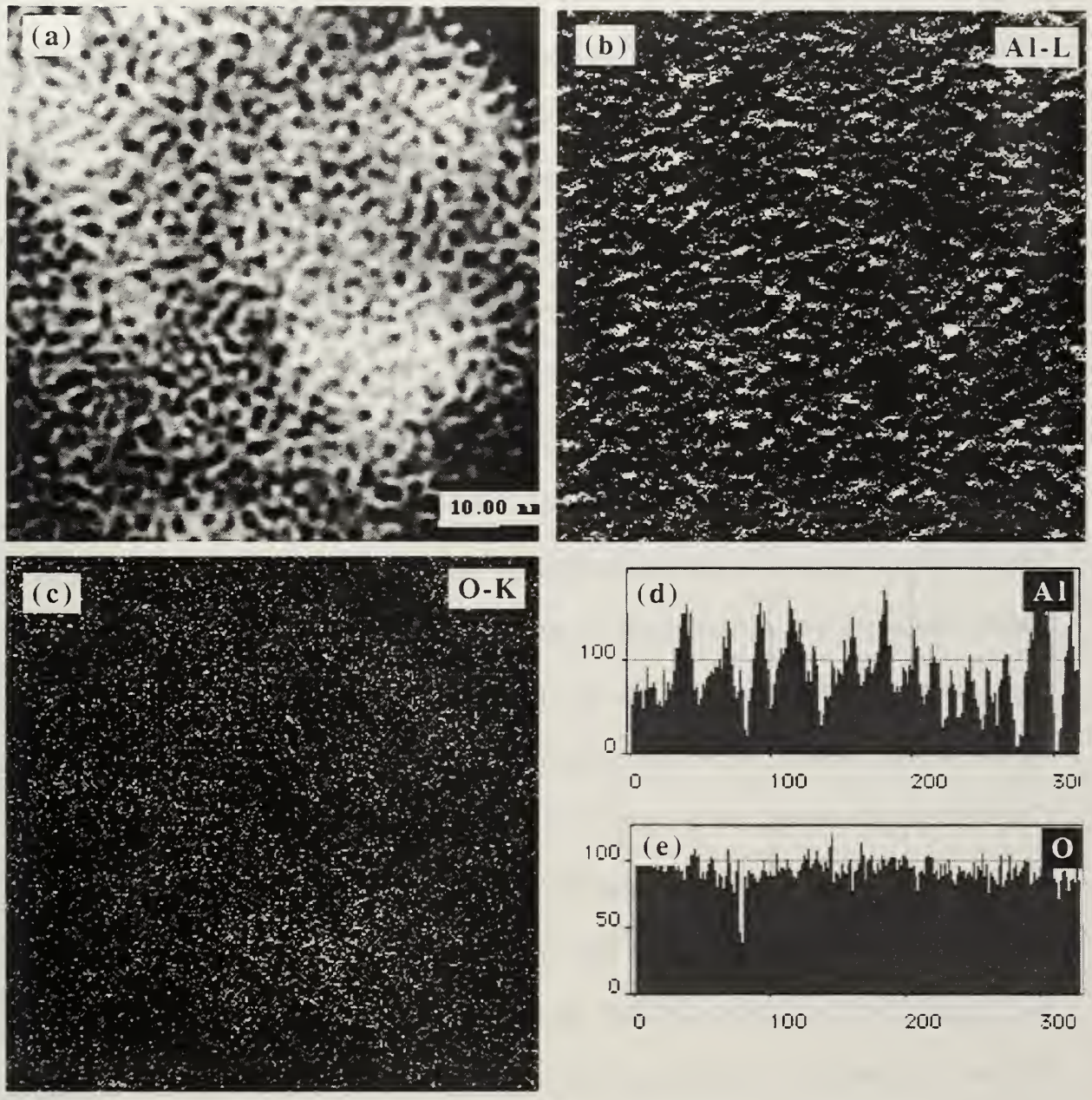

Figure 19: Alumina/Cr film, annealed, showing (a) crystals of the alumina rich phase in the chromia rich phase; (b) Al elemental map; (c) O elemental map; (d) Al profile; (e) O profile. Profiles shown in (d) and (e) were obtained along a randomly drawn rectangle.

Figures 18a and 18b show significant inter-diffusion of the metallization and the Al_2O_3. There is also significant interdiffusion seen across the interface of C and Cr. The C and Cr phase diagram [Ref. 21] shows that there are three intermediate chromium carbide phases in the solid state – $Cr_{23}C_6$, Cr_7C_3, and Cr_3C_2. The presence of one or more of these carbides would suggest that the strength of the interface would be very high since both inter-diffusion and chemical bonding were present. Auger spectra obtained from the interfacial carbide layer (Figure 20) were compared with spectra for the individual carbide phases available in the literature [Ref. 22]. These spectra are reproduced in Figures 21a and 21b, along with a blow-up of the C and Cr regions of the Auger spectrum of the Cr-diamond interface in the present sample (Figure 21c) and a spectrum from diamond (Figure 21d). The primary difference between diamond and carbide Auger electron spectra signals is the absence of the 252eV (KL_1L_1) and 260eV (KL_1L_2) transition peaks in diamond. In Figure 20, peaks corresponding to the KL_1L_1 and KL_1L_2 transitions in carbide are seen, indicating that there must be a carbide at the Cr/CVDD interface after heat treatments. The Auger peak to peak height ratio of $I_{C(271\ eV)}/I_{Cr(489\ eV)}$ is used to determine which of the three chromium carbides is present. The C signal from diamond, which contains only one minima at 272 eV, was superimposed on the C signal from the carbide; therefore, accurate peak to peak height ratios could not be obtained. Comparison of the fine features of the collected C peak with those of $Cr_{23}C_6$ [Ref. 23] and Cr_3C_2 [Ref. 24] revealed that the Cr_3C_2 carbide is unlikely since it contains two doublets that were not present in the collected peak. Investigation of the fine features associated with the Cr signal showed that the 489 eV and 529 eV minima peak heights are the same for metallic Cr but in the surveys obtained in this work (Figure 21c), the 529

eV minima peak was smaller than the 489 eV minima peak. This feature was also present in the spectra presented in Reference 22 (Figure 1). Calculations of the free energy of formation (ΔG) [Ref. 25] showed that of the three carbides, $Cr_{23}C_6$ has the lowest ΔG [–85,898 calories/mole at the annealing temperature (400 °C) and –94,593 calories/mole at the peak firing temperature (840 °C) of the Au paste compared with –42,424/-46,607 calories/mole and –21,614/-23,597 calories/mole for Cr_7C_3 and Cr_3C_2, respectively] making it the thermodynamically most stable of the 3 phases. The combination of the thermodynamic data and the Auger spectral analysis suggests that $Cr_{23}C_6$ is the carbide species formed at the interface. The presence of the chromium carbide provides chemical bonding at the interface and results in strong adhesion between the overlying Al_2O_3/Cr_2O_3 layer and the underlying diamond.

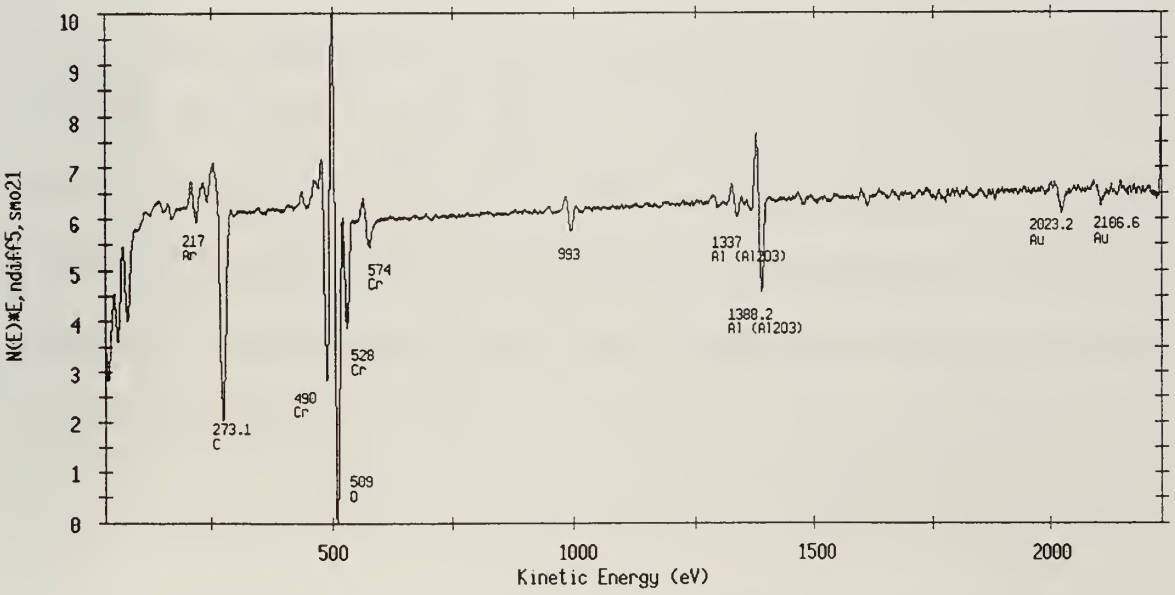

Figure 20: AES Survey from interfacial carbide layer of Au-metallization on CVDD with Al_2O_3/Cr inter-layer.

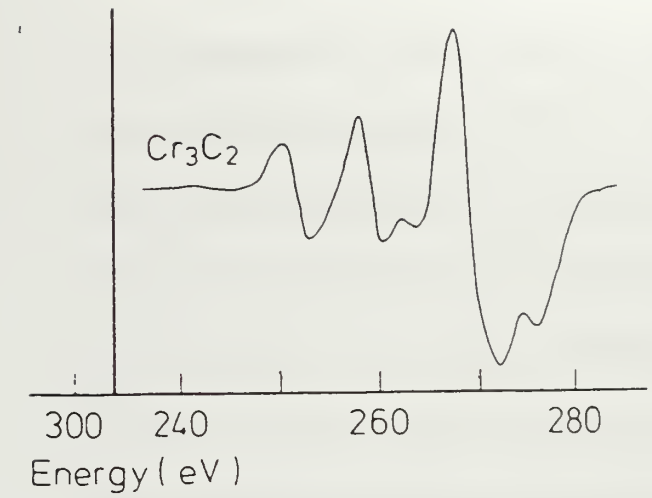

(a)

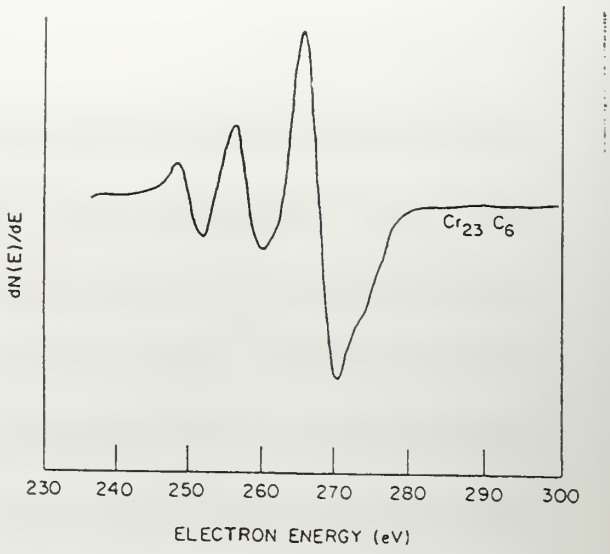

(b)

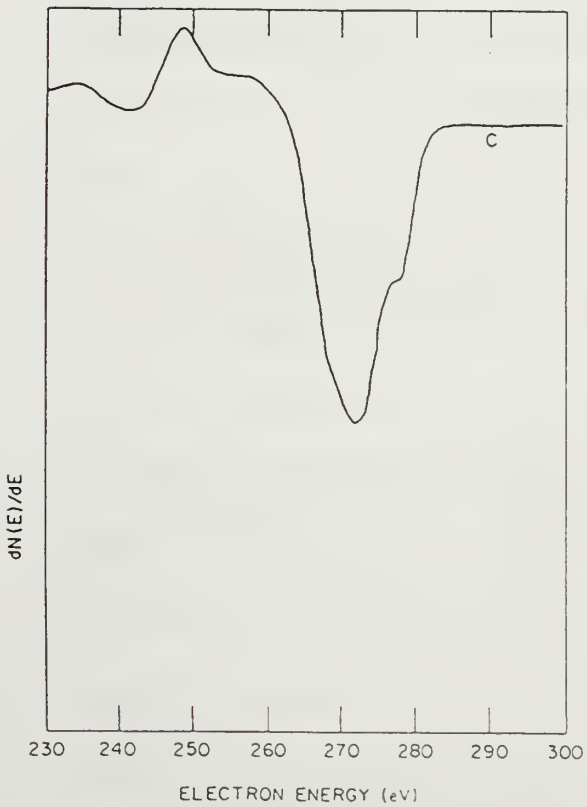

(c)

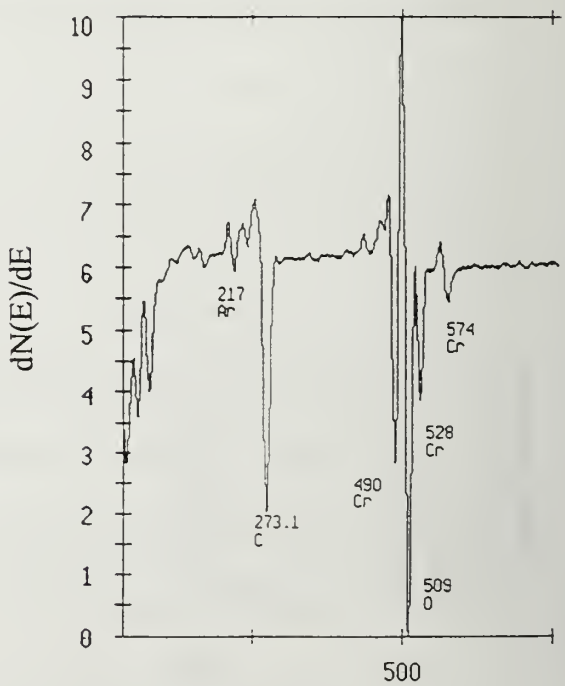

(d)

Figure 21: (a) Cr_3C_2 Auger [Ref. 24]; (b) $Cr_{23}C_6$ Auger peaks [Ref. 22]; (c) CVD diamond Auger peaks [Ref. 26]; and (d) C-Cr Auger peaks from Au-metallized CVDD with Cr/Al_2O_3 inter-layer

Figure 22a shows a cross-sectional TEM micrograph of a diamond substrate metallized with Au using a Al_2O_3/Cr inter-layer. Region A represents the CVDD substrate, region B comprises the interfacial Al_2O_3/Cr layer as well as segregated glassy phases from the frits contained in the metallization, and region C represents the Au metal. The composition across the layers was analyzed using EDXS with very fine (6nm and 4nm) probe sizes with spectra taken from well within the CVD diamond to well within the Au region. The EDX spectrum from the crystallites at the interface between region A and B shows Cr and C, suggesting the presence of the chromium carbide. No C was detected anywhere else in region B, suggesting that diffusion of C is limited to the formation of the interfacial carbide crystallites. The spectrum taken immediately adjacent to the crystallite structure showed only Cr indicating that there is a region of metallic chromium remaining even after firing the Au-metallization at 840 °C. The spectrum from the middle of the interlayer (Figure 22c) shows the expected presence of Al and O as well as showing that the thick paste frits (Bi, Si, Zn, and Cu) have diffused approximately half way through the inter-layer. Figure 22d is the spectrum from the glassy-phase region close to the B-C interface, showing segregation of the Si and Cu containing frits to the interface. A comparison of all of the EDX spectra across region B reveals that it is compositionally graded with Cr having diffused through approximately half the Al_2O_3 layer.

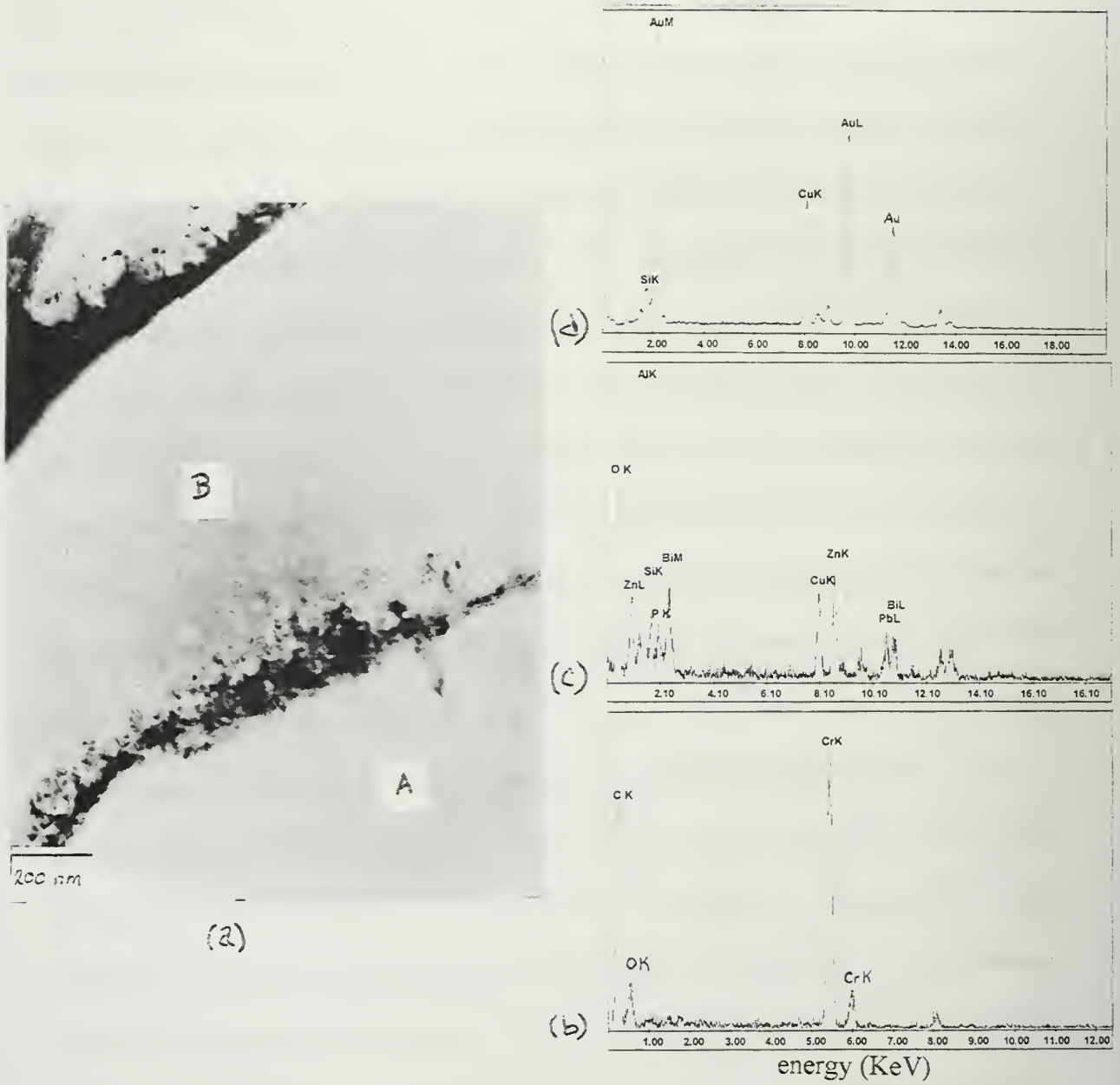

Figure 22: Cross-sectional TEM micrograph. Region A represents the CVDD substrate, region B comprises the Al_2O_3/Cr layer as well as segregated glassy phases from the frits contained in the metallization, and region C represents the Au metal. EDX spectra from (b) interface between regions B and C; (c) mid-point of region C; and (d) region containing C-Cr crystallites at the interface between regions B and A.

D. EMBRITTLEMENT OF Au BY Pb-Sn SOLDER: A FAILURE ANALYSIS

An attempt was made to test the strength of the interface between CVDD and the Au metallization by pull testing samples with and without the Al_2O_3/Cr inter-layer in accordance with MIL-M-28787D [Ref. 27]. As discussed earlier (section III-B), the standard requires attaching a Cu wire to the pads and the metallization by a Pb-Sn solder. However, during soldering of the Cu wire to the Au metallization, the metallization underwent chemical degradation and resulted in premature failure prior to testing. This precluded obtaining valid measurements of the adhesive strength of CVDD-Au interfaces.

An SEM analysis of the fracture surface of the pads which decohered from the substrate surface revealed Pb and Sn from the solder have diffused a substantial distance into the Au pad and formed brittle intermetallic compounds. EDXS (Figure 23a and 23b) of the fracture surface of two of the pads revealed segregation of Pb and Sn at several near-grain boundary regions, suggesting that Pb and Sn diffused along the Au grain boundaries and possibly formed Sn-Au and Pb-Au intermetallics. Because of this embrittlement of the metallization pads during soldering, no quantitative data on the impact of the Al_2O_3/Cr inter-layer could be obtained.

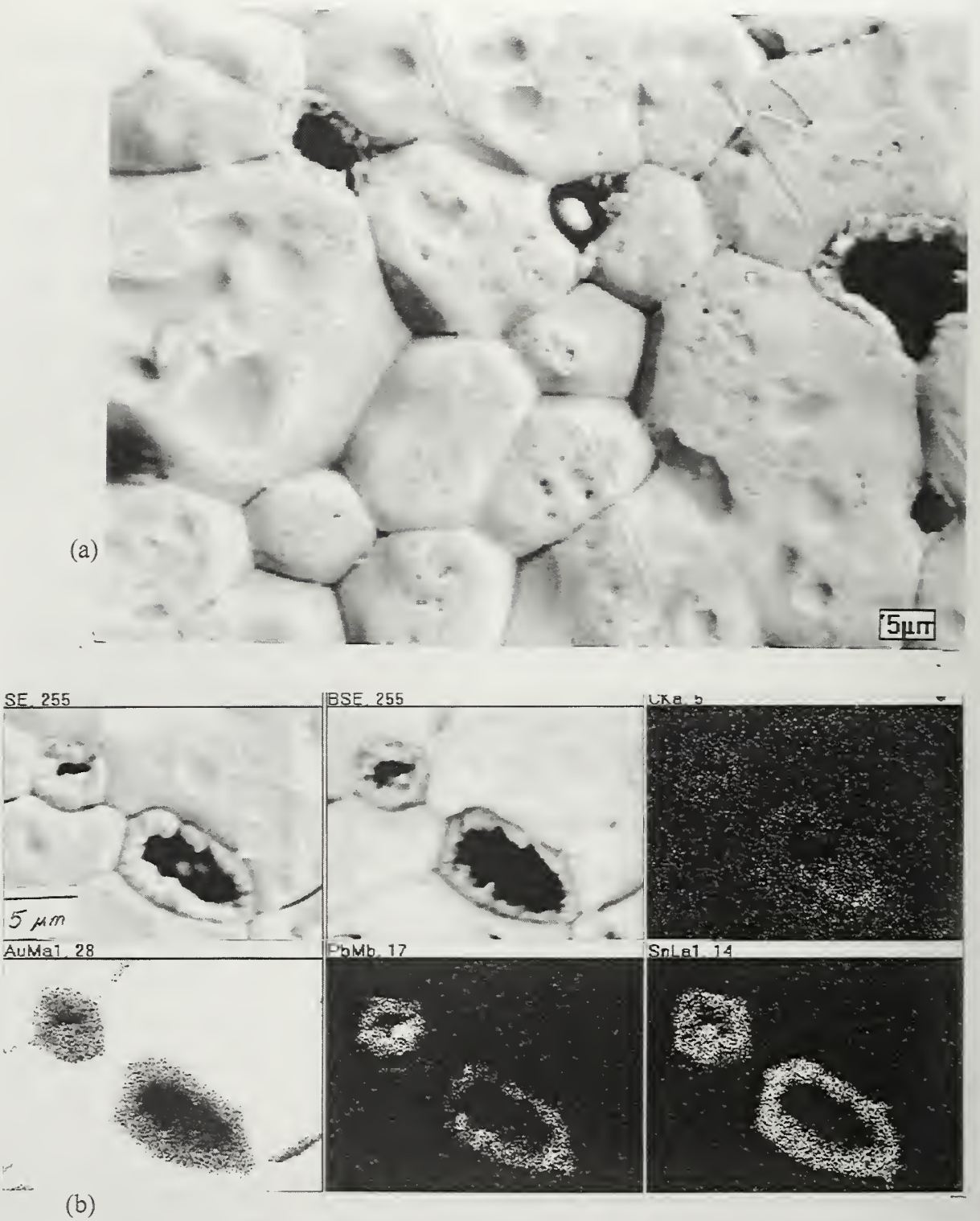

Figure 23: (a) Secondary electron image and (b) X-ray images of fracture surface of two Au pads revealing segregation of Pb and Sn at several near grain boundary regions.

V. SUMMARY AND CONCLUSIONS

Metallization of CVD diamond by commercially available Ag and Au pastes was conducted. The effect of a Al_2O_3/Cr intermediate layer between the metallization and the CVD diamond was evaluated. This study shows that incorporation of an intermediate layer (Cr/Al_2O_3) results in chemical bonding both with the underlying diamond substrate and the overlying Au/Ag metallization. The chemistry and the microstructure of the interface were characterized in detail by AES, SEM, EDXS and TEM, and it was found that:

1. there is interdiffusion of C and Cr at the Cr/CVD diamond interface, leading to the formation of fine crystallites of a chromium-carbide (most likely $Cr_{23}C_6$)
2. above the Cr-carbide layer, a metallic Cr layer was observed
3. during the process of depositing the Al_2O_3/Cr inter-layer and the subsequent anneal, Cr and O chemically combine to form chromium oxide, which then diffuses into the Al_2O_3 layer to give rise to a very fine structure consisting of Cr_2O_3-rich and Al_2O_3-rich regions with nanometer scale spatial composition modulation
4. the frits contained in the metallization paste melt during firing and segregate at the metallization/Al_2O_3 interface, producing an oxide rich interfacial region with through thickness composition variation resulting from different extents of gravitational settling of melts of different specific gravity and/or various extents of solid-state diffusion of the different elements present in the frit through the Al_2O_3 intermediate layer.

Based on the above, it is the conclusion of this thesis that CVDD may be effectively metallized by commercial thick pastes by using a Cr/Al_2O_3 inter-layer which produces excellent chemical bonding across the metal/glassy phases/Al_2O_3/Cr/CVDD interfaces. Further studies need to be conducted in characterizing the mechanical

strength of the interfaces, and in determing the electrical properties of the Al_2O_3/Cr modified CVDD substrate surface in order to determine the efficacy of the proposed approach for use in electronics packaging.

REFERENCES

1. E. S. K. Menon and I. Dutta, Appl. Phys. Lett. 68 (21), 20 May 1996.

2. Microelectronics Packaging Handbook, edited by R. R. Tummala and E. J. Rymaszewski, Van Nostrand Reinhold, New York, 1989 pp. 1.

3. J. J. Licari, Multichip Module Design, Fabrication, & Testing, McGraw-Hill Inc., New York, (1995) pp. 144.

4. B. V. Spitsyn and B. V. Derjaguin: USSR Inv. Certif., No. 339134, (1956). From B. V. Spitsyn, L. L. Bouilov and B. V. Derjaguin: Vapor Growth of Diamond on Diamond and Other Surfaces, J. Crystal Growth, 52, (1981) pp. 219.

5. Study on Diamond: National Institute for Research in Inorganic Materials of Japan, Research Report, 20, (1979) pp. 64.

6. J.K. Hagge, IEEE Trans. Compon., Hybrids Manuf. Technol., 15(1) (1992) pp. 29-39.

7. C. D. Iacovangelo and E. C. Jerabek, *Proceeding of the International Symposium on Microelectronics, 1993* (The Microelectronics Society, 1993), Vol. 2105, pp. 132.

8. C. D. Iacovangelo, P. J. DiConza, E. C. Jerabek, and K. P. Zarnoch, Mater. Res. Soc. Symp. Proc. 337, 401 (1994).

9. Y. S. Chung and H. Kim, "Effect of Oxide Glass on the Sintering Behavior and Electrical Properties in Ag Thick Films," IEEE Trans. On Components, Hybrids, and Manufacturing Tech., vol. 11, no. 2, pp. 195-199, June 1988.

10. B. Chiou, K. C. Liu, J. Duh, and M. C. Chung, "Role of Glass on the Microstructure Evolution of a Thick-Film Dielectric," IEEE Trans. On Components, Hybrids, and Manufacturing Tech., vol. 14, no. 3, pp. 645, September 1991.

11. R. E. Hoffman and D. J. Turnbull, "Lattice and grain-boundary self-diffusion in silver," J. Appl. Phys., vol. 22, no. 5, pp. 634-639, 1950.

12. V. R. Howes, "Graphitization of diamond, "Proc. Phys. Soc., Vol. 80, No. 3., (1962) pp. 648-662.

13. T. Evans and R. James, "A study of the transformation of diamond to graphite," J. Proc. Roy. Soc. A, Vol. 277, No. 1369, (1964), pp. 260-269.

14. Diamond Films and Coatings Development, Properties, and Applications, edited by Robert F. Davis, Noyes Publications, New Jersey (1993) pp. 14-15.

15. E. S. K. Menon and I. Dutta, Appl. Phys. Lett. 68 (21), 20 May 1996.

16. F. G. Foster, "Embrittlement of solder by gold from plated surfaces," Papers on Soldering, McGraw Hill, 1972, pp. 13-19.

17. J. I. Goldstein, D. E. Newbury, P. Echlin, D. C. Joy, A. D. Romig, Jr., C. E. Lyman, C. Fiori, and E. Lifshin, Scanning Electron Microscopy and X-ray Microanalysis – A Text for Biologists, Materials Scientists, and Geologists, 2nd Ed. Plenum Press, New York, 1994 pg. 131.

18. E. N. Bunting, *Bur. Standards J. Research*, 6[6] 648 (1931); R. P. 317.

19. D. M. Roy and R. E. Barks, *Nature* (London), 235 [58] 118 (1972).

20. E.S.K. Menon and I. Dutta, unpublished research.

21. Binary Alloy Phase Diagrams, M. Venkatraman, J. P. Neumann, 1990, pp. 838.

22. S. Danyluk, J. Y. Park, D. E. Busch, "Auger Electron Spectroscopy of Stoichiometric Chromium Carbides and Carbide Precipitates at Grain Boundaries of Type 304 Stainless Steel", Scripta Metallurgica, Vol. 13, pp. 857-862, 1979.

23. Ibid. pg. 861.

24. Practical Surface Analysis 2nd Ed. Volume 1-Auger and X-ray Photoelectron Spectroscopy, Edited by D. Briggs, M. P. Seah, John Wiley and Sons, New York, 1996, pp. 102.

25. E. T. Turkdogan, Physical Chemistry of High Temperature Technology, Academic Press, New York, (1980) pg. 10.

26. M. L. Terranova, V. Sessa, R. Bernardini, I Davoli, M. De Crescenzi, "Local structure of diamond films: Auger and EELFS investigation," *Surface Science* 331-333 (1995) 1050-1055.

27. Government/Military Standards and Specifications Service, "Military Specification Modules, Standard Electronic General Specification For," (MIL-M-28787D, Information Handling Services, Englewook, CO, 30 March 1989), microfiche.

INITIAL DISTRIBUTION LIST

1. Defense Technical Information Center 2
   8725 John J. Kingman Rd., STE 0944
   Ft. Belvoir, Virginia 22060-6218

2. Dudley Knox Library 2
   Naval Postgraduate School
   411 Dyer Rd.
   Monterey, California 93943-5101

3. Commanding Officer 1
   Naval Air Warfare Center
   Aircraft Division – Indianapolis
   Code B816 (Attn: Dr. J. Sosniak)
   6000 East 21st St.
   Indianapolis, Indiana 46218-2189

4. Commanding Officer 1
   Naval Surface Warfare Center – Crane Division
   Code 6043 (Attn: Chris Sims)
   Crane, Indiana 47522-5001

5. Crystallume Corporation 1
   Dr. Michael Drory
   3506 Basset Street
   Santa Clara, CA 95054

6. Commanding Officer 1
   Naval Surface Warfare Center – Crane Division
   Code 6043 (Attn: Kevin Beasley)
   Crane, Indiana 47522-5001

7. Norton Diamond Film 1
   Phil Fabis
   Goddard Road
   Northboro, Massachusetts 01532

8. Dr. Pehr Pehrsson 1
   Code 6174, Chemistry Division
   Naval Research Laboratory
   Washington, D.C. 20375-5342

9. Dr. Indranath Dutta, Code ME/Du 1
Naval Postgraduate School
700 Dyer Rd.
Monterey, California 93943-5101

10. Dr. Sarath Menon, Code ME/Ms 1
Naval Postgraduate School
700 Dyer Rd.
Monterey, California 93943-5101

11. LT. Darwin Kroll 3
P.O. Box 113
Millington, Michigan 48746

DUDLEY KNOX LIBRARY
NAVAL POSTGRADUATE SCHOOL
MONTEREY CA 93943-5101

DUDLEY KNOX LIBRARY
3 2768 00336052 0